Annu. Rev. Earth Planet. Sci. 1998. 26:219–53

SATELLITE ALTIMETRY, THE MARINE GEOID, AND THE OCEANIC GENERAL CIRCULATION

Carl Wunsch and Detlef Stammer
Department of Earth, Atmospheric, and Planetary Sciences, Massachusetts Institute of Technology, Cambridge, Massachussetts 02139; e-mail: cwunsch@pond.mit.edu, detlef@lagoon.mit.edu

KEY WORDS: geodesy, gravity, climate

ABSTRACT

For technical reasons, the general circulation of the ocean has historically been treated as a steady, laminar flow field. The recent availability of extremely high-accuracy and high-precision satellite altimetry has provided a graphic demonstration that the ocean is actually a rapidly time-evolving turbulent flow field. To render the observations quantitatively useful for oceanographic purposes has required order of magnitude improvements in a number of fields, including orbit dynamics, gravity field estimation, and atmospheric variability. With five years of very high-quality data now available, the nature of oceanic variability on all space and time scales is emerging, including new findings about such diverse and important phenomena as mixing coefficients, the frequency/wavenumber spectrum, and turbulent cascades. Because the surface elevation is both a cause and consequence of motions deep within the water column, oceanographers soon will be able to provide general circulation numerical models tested against and then combined with the altimeter data. These will be complete three-dimensional time-evolving estimates of the ocean circulation, permitting greatly improved estimates of oceanic heat, carbon, and other property fluxes.

INTRODUCTION

The most fundamental obstacles to determining the oceanic general circulation lie with its opacity to electromagnetic radiation and the volume of fluid it is necessary to observe, relative to the speed and costs of oceanographic vessels.

0084-6597/98/0515-0219$08.00

The electromagnetic opacity forces one to place instruments physically at the location of a desired measurement, and the ships necessary for deployment have been the fundamental observational tool. Fortunately for oceanographers, many features of the circulation, in particular the distribution of scalar fields such as temperature or oxygen distribution, exhibit permanent large-scale structures. This temporal stability has permitted the combination of observations obtained over decades into large-scale charts and the interpretation of these "tracers" in terms of large-scale temporally stable flow fields, for example the large-scale structure seen in Figure 1*a*. The intellectual framework of general ocean circulation physics and chemistry has thus rested fundamentally on the hypothesis that the fluid dynamics was that of a nearly steady, laminar system. This interpretation has reached its apotheosis in the conceptual reduction of the system to a "global conveyor belt."

In practice, however, it was known almost from the beginnings of the subject (e.g. Helland-Hansen & Nansen 1920) that the ocean was constantly changing. By the middle of the 1970s, it had become clear that the system was, in a basic sense, turbulent. Figure 1*b* shows one component of the fluid transport, as estimated by Macdonald (1995), lying between about 200 and 1000 m in the Pacific Ocean during a particular ship crossing, and Figure 1*c* depicts the hodograph from a two-year current meter record. The extremely variable flow is unlikely to be a purely passive "noise" in which only some hypothetical long-term average field governs the oceanic circulation. Large-scale features can easily be the consequence of the complex smaller scale, rapidly time-evolving flows, with their Lagrangian summations in space and time producing the observed structures. If the latter depiction is more correct, purely ship-based observations can never produce observations adequate to understand the overall physics (or chemistry and biology) of the system.

By the late 1970s, the rise of concern about climate change was also leading to the demand from a wider community for prediction of future oceanic states. Because predictions of turbulent fluids depend directly upon accurate initial conditions, the question of how to observe the global-scale, turbulent system became urgent.

Space-based techniques are an obvious choice when studying a global-scale fluid. Unfortunately, the electromagnetic opacity means that all measurements of the ocean from above the sea surface are restricted to properties at or near the sea surface itself: skin temperature, color, dielectric constant, scattering cross-section, etc. [So-called extremely low-frequency radiation (ELF) does penetrate the ocean, but at wavelengths and frequencies useless for the transmittal of information.] Unfortunately, the relationship between these measured surface properties and the fluid flow at depth is complicated, indirect, and weak. Thus, measurements of properties such as the surface temperature have contributed in only

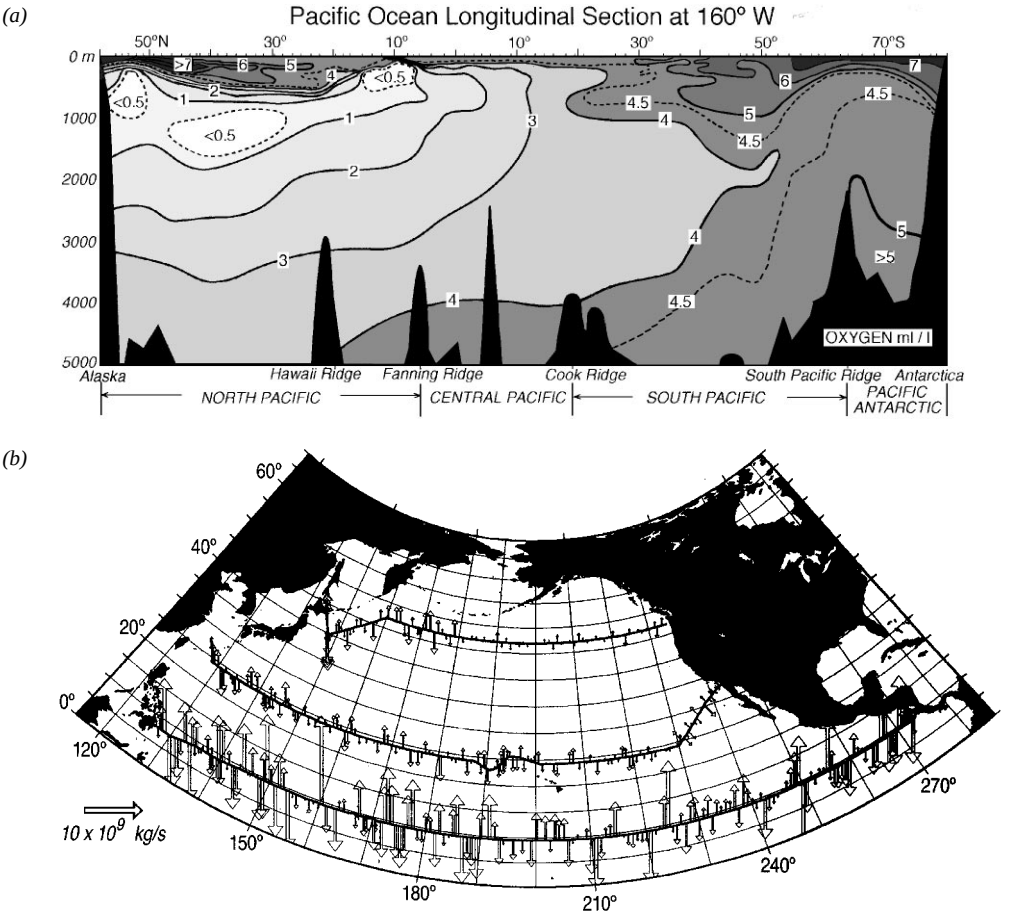

Figure 1 (*a*) A section (after Dietrich et al 1975) showing the large-scale patterns of oxygen concentration in a section running meridionally through the Pacific Ocean. These patterns have traditionally been interpreted to imply the dominance of a simple, large-scale, nearly unchanging flow field. (*b*) Instantaneous mass transports in the depth range roughly between 200 and 1000 m perpendicular to the three ship tracks, as estimated by Macdonald (1995). The very large spatial variability (and an implied temporal variability) undermines the idea that a simple laminar flow field produces the large-scale oceanic property distributions. (*c*) Hodograph plot (meridional component of velocity, v, as a function of the zonal component, u) from two years of daily average velocities from a current-meter record at 41°N, 175°W, 135-m depth, in the North Pacific Ocean. The lack of temporal stability is evident.

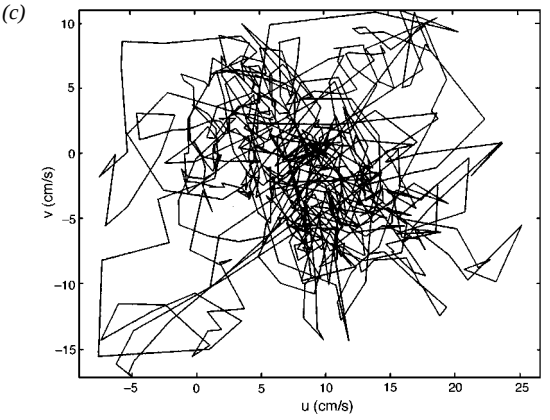

Figure 1 (*Continued*)

minor ways to understanding of the circulation itself. (Surface temperature is very important, however, as a boundary condition for the overlying atmosphere.)

When searching for a physical property of the sea surface that directly reflects the three-dimensional, large-scale fluid flow, only the surface elevation emerges as a serious candidate. Consider that for oceanic flows on spatial scales exceeding a few tens of kilometers, the hydrostatic approximation is a good one. In a coordinate system (θ, λ, z), where θ is colatitude and λ is longitude, let $z = 0$ be a local gravitational equipotential defining the sea surface with the ocean at rest. Then any motion of the ocean generates a hypothetically measurable deflection of the sea surface, $z = \eta(\theta, \lambda, t)$ (see Figure 2), such that the hydrostatic pressure perturbation at $z = 0$ is

$$p_s(\theta, \lambda, t) = g\rho\eta(\theta, \lambda, t), \tag{1}$$

where ρ is the fluid density and g is the local gravitational acceleration. Variations in ρ at the sea surface can be ignored for present purposes. Use of Equation 1 for understanding large-scale oceanic motions depends upon the demonstration that oceanic motions on time scales exceeding a few days and on spatial scales exceeding about 50 km do not form pressure boundary layers at the sea surface. To the contrary, simple theory shows that elevations η on these time and space scales reflect motions deep within the ocean rather than surface motions per se—in contrast with all other known surface properties. (A simple analogy to this idea can be obtained from contemplating the movement of fluid in a stirred cup of coffee. When the coffee has been set spinning, a knowledge of the shape of the fluid surface plus some simple fluid dynamics permits one to calculate the three-dimensional flow in the cup in detail, including the motion in

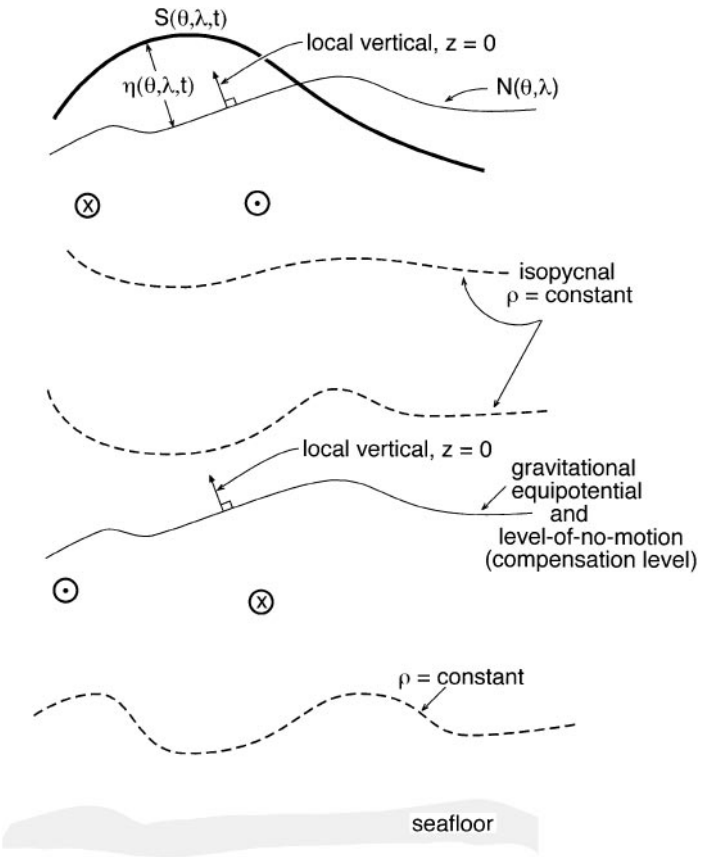

Figure 2 Schematic (not to scale) of the relationship between the sea surface elevation S, the geoid height N, and the oceanic density field. If the elevation changes, η, in S relative to N, are compensated by interior density gradients, one can produce a level-of-no-motion at depth. Generally speaking, the sense of the flow would reverse below this depth. Directions of flow are appropriate to the northern hemisphere. Note that N is usually described as the deviation from the underlying reference ellipsoid, E, but then notation often omits specific reference to the difference between N and the true geoid height $N + E$.

sidewall and bottom viscous boundary layers, with considerable accuracy. The equations governing the ocean circulation are more complex than for a coffee cup, but the basic principle is identical.)

A corollary is equally important: Near-surface velocity boundary layers do not form pressure boundary layers. In particular, the intense, near-surface directly wind-driven oceanic flow, which is idealized as an Ekman layer (see e.g. Gill 1982), is invisible to the altimeter. Thus, η reflects only that component

of the circulation extending to great depth in the ocean; flows confined near the sea surface are unseen by devices measuring the elevation. (The effect of the Ekman layer on the surface pressure signal needs to be reconsidered in the presence of mean surface currents with strong shear.)

In this review, we outline the basic physical considerations of satellite altimetry and describe the major results to date concerning the oceanic general circulation. The subject is unique perhaps in the breadth of physical elements affecting the measurement accuracy and precision, and thus satellite altimetry has brought with it progress in many areas of geodesy, geophysics, meteorology, orbit physics, etc, which we can only touch on in passing. The literature is already too large for us to attempt a comprehensive discussion of all relevant papers, and because of the comparatively recent acquisition of long altimetric records, some of the most interesting work is still in progress. A more extended discussion of the fundamentals can be found in books by Stewart (1985) or Rummel & Sansò (1993).

DYNAMICAL PRELIMINARY

Information about the ocean circulation contained in η can be understood and exploited in a number of ways that vary greatly in their sophistication. The ocean contains many dynamical regimes, each of which has to be considered separately. To keep this review finite, we focus on the regime representing the open ocean circulation, defined here roughly as describing the ocean in water of depths exceeding about 1000 m, on spatial scales larger than about 30 km (there is some latitudinal dependence), with persistence times exceeding about one day, at latitudes poleward of about 3°. Such motions are nearly geostrophic—meaning that there is a close balance between the Coriolis force and the pressure force, written as

$$2\Omega \sin\phi \rho v(\phi, \lambda, z = 0) = \frac{g\rho}{a \cos\phi} \frac{\partial \eta(\phi, \lambda)}{\partial \lambda}, \tag{2}$$

$$-2\Omega \sin\phi \rho u(\phi, \lambda, z = 0) = \frac{g\rho}{a} \frac{\partial \eta(\phi, \lambda)}{\partial \phi}, \tag{3}$$

where a is the Earth's mean radius, Ω is the mean Earth rotation rate, z is the local vertical coordinate, $\phi = \pi/2 - \theta$ is latitude, and λ is again longitude. u is the flow component directed zonally and v meridionally. That is, as long as $|\phi|$ exceeds about 3°, the sea surface slope predicts the oceanic surface velocity well, and vice-versa (3° distance from the equator is only a rough guideline—dependent on the noise level; geostrophic balance appears to be valid much closer to the equator). At 30° latitude, 1-cm change in η over a lateral distance

of 100 km produces a surface flow velocity of about 1 cm/s. Equations 2 and 3 show that it is only the lateral gradient of sea surface elevation that is of dynamical significance—not the elevation itself.[1]

The velocity implies a mass flux. Consider the meridional component of mass transport between two longitudes, λ_1 and λ_2, assuming the hydrostatic pressure gradient extends to the seafloor, $z = -d$, so that u,v are depth independent:

$$\begin{aligned} T_v &\equiv \int_{-d}^{\eta} \left\{ \int_{\lambda_1}^{\lambda_2} \rho v(\phi, \lambda, z)\, a \cos\phi d\lambda \right\} dz \\ &= g\rho d \int_{\lambda_1}^{\lambda_2} \frac{1}{a 2\Omega \sin\phi \cos\phi} \frac{\partial \eta}{\partial \lambda} a \cos\phi d\lambda \\ &= \frac{g\rho d}{2\Omega \sin\phi} \left(\eta(\lambda_2, \phi) - \eta(\lambda_1, \phi)\right) \end{aligned} \tag{4}$$

(assuming $|\eta| \ll d$). A similar expression exists for the zonal transport, with the slight complication of the meridional dependence of the Coriolis force through $2\Omega \sin\phi$. It is an important peculiarity of geostrophic balance in an ocean of uniform depth that the mass flux depends only on the elevation change, $\Delta\eta$, and the water depth and not the distance over which it occurs. If $d \approx 4000$ m and with $\Delta\eta = 1$ cm, the total mass of fluid moving is about 7×10^9 kg/s [about 7 Sverdrups (Sv) in the oceanographic unit of volume flux such that 1 m^3 of mass is nearly 10^3 kg]. To provide a context, the mass flux of the Gulf Stream at Florida is about 30 Sv, rising to about 70 Sv near Cape Hatteras. So, a 1-cm elevation change represents a significant movement of water. But because something is already known about the ocean circulation, the measure of the utility of satellite altimetry is the degree to which it provides new information, not its redundant measure of what is already known. Wunsch (1981a) estimated that the time-average circulation was already known to the equivalent of 10–25 cm over spatial scales ranging from 30–10,000 km. Thus, it appeared that altimetry would provide much new information only if it could achieve absolute accuracies approaching 1 cm. This measure of accuracy is over-simplified—in particular, it speaks neither to the large-scale time-dependent components that were essentially completely unknown, nor to the complex scale and geographical dependence—but it proves useful in practice.

[1]Analogous, but different, analyses can be constructed for the three other major dynamical regimes: the equatorial region, continental shelves and other shallow water, and high-frequency motions with periods shorter than about $1/(2\Omega \sin\phi)$. Each of these deserves its own review. The crucial issue is to have a dynamical model, no matter how complex, that permits computation of the flow field from the known elevation η. Geostrophic balance Equations 2 and 3 are a particularly simple example of such a model. Similar models can be constructed, e.g. for gravity waves in deep or shallow water, and altimetry can be used in many different physical situations.

The assumption that the large-scale pressure gradient extends unattenuated to the seafloor is also oversimplified. It would be true always if the ocean were of uniform density ρ. In practice, surface elevation changes are often found to be partially "compensated," in the geophysical terminology, by density adjustment at depth (Figure 2), so that the horizontal pressure gradients could vanish at some depth $z = z_c(\phi, \lambda)$. In a stratified ocean, an important parameter is the local vertical derivative of the density field $\partial\rho/\partial z$, usually measured as the "buoyancy frequency" defined as

$$N_b(z) = \left[-\frac{g}{\rho(\phi, \lambda, z)} \frac{\partial \rho(\phi, \lambda, z)}{\partial z} \right]^{1/2}. \tag{5}$$

Then it is a matter of simple fluid dynamics to show that density compensation of a surface elevation change over lateral distance L can occur only on a vertical scale of order

$$H \approx \frac{2\Omega \sin \phi L}{N_b}. \tag{6}$$

Away from the tropics, typical oceanic values for H are 2–3 km if L is greater than about 100 km. Equation 6 has to be modified where there is a strong background oceanic flow, at low latitudes (see e.g. Gill 1982 or Pedlosky 1987), and for so-called steric effects. These last arise from local exchanges with the atmosphere of heat and fresh water, primarily on basin-wide scales at the annual period, and are compensated within about 100 m of the sea surface. But the basic conclusion is that surface pressure gradients at long wavelengths and low frequencies reflect oceanic motions at several kilometers depth and, if uncompensated, right to the seafloor.

BASIC OBSERVATIONAL ELEMENTS

The fundamental geometry of space-borne altimetry is seen in Figure 3. A radar altimeter is flown at radius $H(\theta, \lambda, t)$ and determines the distance $h(\theta, \lambda, t)$ from the spacecraft to the physical sea surface by measuring the nadir round-trip travel time of a pulse emitted and received by the radar. If $H(\theta, \lambda, t)$ is known, then the elevation of the sea surface relative to the center of the Earth, $S(\theta, \lambda, t)$ is obtained as

$$S(\theta, \lambda, t) = H(\theta, \lambda, t) - h(\theta, \lambda, t). \tag{7}$$

If the ocean were at rest, $S(\theta, \lambda, t)$ would correspond to a gravitational plus centrifugal equipotential at radius $r_g(\theta, \lambda) = N(\theta, \lambda) + E(\theta, \lambda)$, the "geoid height," where E is a reference ellipsoid (Heiskanen & Moritz 1967). As in

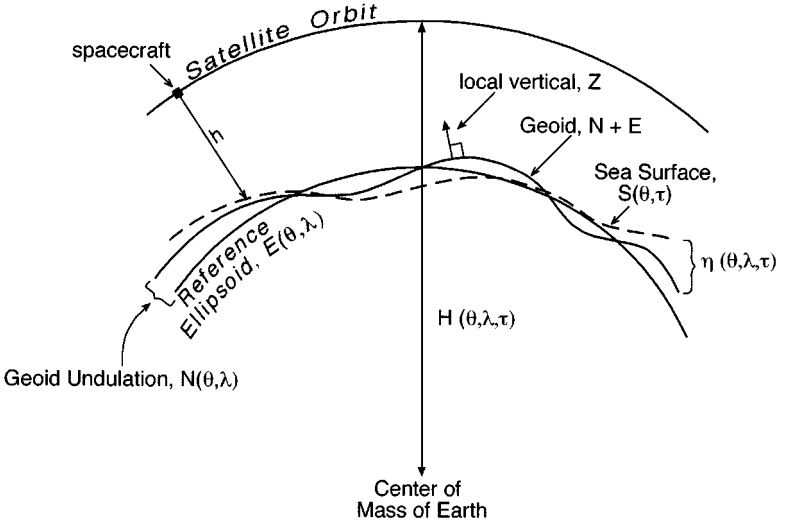

Figure 3 Definition sketch of the geometry of the altimetric measurement of the sea surface topography.

much of the literature, we generally absorb E into N, so the difference,

$$\begin{aligned}\eta(\theta, \lambda, t) &= S(\theta, \lambda, t) - N(\theta, \lambda, t) \\ &= H(\theta, \lambda, t) - N(\theta, \lambda, t) - h(\theta, \lambda, t)\,,\end{aligned} \tag{8}$$

is the desired oceanic surface elevation relative to the geoid height. Note that the geoid itself is a gravitational equipotential value, whereas the geoid height is an elevation; a common practice, which we follow, is the slightly sloppy reference to N as the geoid.

This concept is attractively simple; in practice, because of the required accuracy, it is the most complex ocean observing system ever designed. For orbit stability, the spacecraft must fly at altitudes near $h \approx 1000$ km above the surface of the Earth. Thus, the differences in Equation 8 must be known to within one part in 10^8, which requires that the orbit radius and $N(\theta, \lambda)$ each be determined at 1 cm accuracy. The measurement of h is made through a murky atmosphere with time-varying components of water vapor and ionospheric free-electron content, which modify the speed of electromagnetic radiation by amounts equivalent to apparent fluctuations in sea level that are large compared to 1 cm. The sea surface itself is a complex three-dimensional conducting stochastic field, whose interaction with the incoming radar pulse greatly alters the pulse between the time it leaves the spacecraft and its return there. These and other problems lead

to a long list of corrections that must be made to the basic measurements, which are summarized below. That such a system is now successfully operating at the 2- to 3-cm level of accuracy on many spatial scales, and is still improving, is a testament to a remarkable engineering and scientific accomplishment of the past 15–20 years.

To use the data, one must have some understanding of the various sources of error. In this review we attempt to provide for the reader an entrée into the literature on the major error elements while retaining our focus on an understanding of the major scientific results to date. No claims to citation completeness are made; in particular we generally omit references to the large halo of gray literature that surrounds all spacecraft, confining ourselves mainly to the most recent discussions that lead a reader into the wider body of previous publications.

SOME HISTORY

The first space-borne altimeter known to us (we do not know what took place in the former Soviet Union) was flown for a few days on Skylab in 1973 (see McGoogan 1975). This mission did little more than show that features in the geoid with amplitudes near 100 m could be observed and that radar altimeters "worked."

The first altimeter to attract serious geodetic attention was flown on GEOS-3 in 1975, at a time when the best marine geoid estimates contained errors of tens of meters. By simply setting $\eta = 0$, Equation 7 produces a geoid estimate $\tilde{N} = \tilde{S}$. With a radial orbit error of roughly 10 m (much greater than $|\eta|$) dominating the system, GEOS-3 usefully improved the geoid estimate but not that of ocean circulation.

The SEASAT mission flew in 1978, but it was ill-fated, failing after only three months in orbit. It did, however, achieve an accuracy, after some years of work with the data, approaching 1–2 m, a significant improvement on GEOS-3 but still inadequate for ocean circulation purposes. A summary of the literature on GEOS-3 and SEASAT is provided by Douglas et al (1987).

Following SEASAT, another mission called GEOSAT was flown by the US Navy's Trident submarine program with the stated purpose of improving knowledge of the geoid, again by simply setting $\eta = 0$. This mission was a classified one, but part of the mission was run in an unclassified mode and ultimately much of the data became publicly available; these proved of sufficient quality to be tantalizing in terms of what an altimetric mission purposely built for ocean circulation studies might do; it also gave a considerable community experience in handling altimetric data. [See Douglas & Cheney (1990), the collections of papers in the *Journal of Geophysical Research* (95, C3, C10, 1990), and Verron (1992) for a discussion of the GEOSAT results.] Although

many results from GEOSAT proved scientifically illuminating (Fu & Cheney 1995) and papers continue to be published using the data, the subsequent flight of the so-called TOPEX/POSEIDON mission carried the technology so much further that we describe GEOSAT results only in passing below. A number of ingenious schemes for error reduction in GEOSAT were developed; some of these will undoubtedly be revived in the future as investigators seek to extract the last bit of information from TOPEX/POSEIDON and its successors.

THE TOPEX/POSEIDON MISSION

Beginnings

In the middle 1970s—even before the flight of SEASAT—a small group of visionaries in France and the United States came to believe that satellite altimetric technology could be significantly improved over what was then possible and, should such improvements be put into practice, that understanding of the ocean circulation would be revolutionized by observing it globally for the first time.[2] Obtaining the required accuracy and precision would necessitate improvements, in some cases by more than an order of magnitude, in all the elements making up the altimetric system: orbit determination, gravity field, atmospheric water vapor, ionospheric electron content, the altimetric instrument itself, geodetic reference frames, ocean and load tides, understanding of surface scattering, etc.

Through more than 12 years of vicissitude, which we pass over in silence, such a mission was designed, approved, and ultimately flown as a joint French–United States effort called TOPEX/POSEIDON.[3] This spacecraft was the first ever launched for the primary purpose of determining the general circulation of the oceans. In the meantime, the European Space Agency had launched its first multi-purpose Environmental Research Satellite (ERS-1), which carried an altimeter (Oriol-Pibernat 1990), but for various reasons, the data quality proved much lower than that of TOPEX/POSEIDON, and the results of the latter mission are the focus of the remainder of this review. Subsequently, some of the problems of ERS-1 were overcome with the 1995 launch of ERS-2, and

[2]For various reasons, the mission statement accepted a design goal of 13 cm (see TOPEX Science Working Group 1981), even though it was widely, if not universally, understood that such an outcome would be disappointing and basically not very useful. In practice, TOPEX/POSEIDON shows that the global root-mean-square (rms) temporal variability is less than 10 cm.

[3]TOPEX is an acronym obtained from Ocean TOPography EXperiment. Contrary to widespread belief, POSEIDON is also an acronym, a dual one in French and English, from M Lefebvre: Premier Observatoire Spatial Étude Intensive Dynamique Ocean et Nivosphere (sic), and Positioning Ocean Solid Earth Ice Dynamics Orbiting Navigator. The inability of the two space agencies to agree on a single, simple name left the cumbersome label as a souvenir of the difficulties of international collaboration.

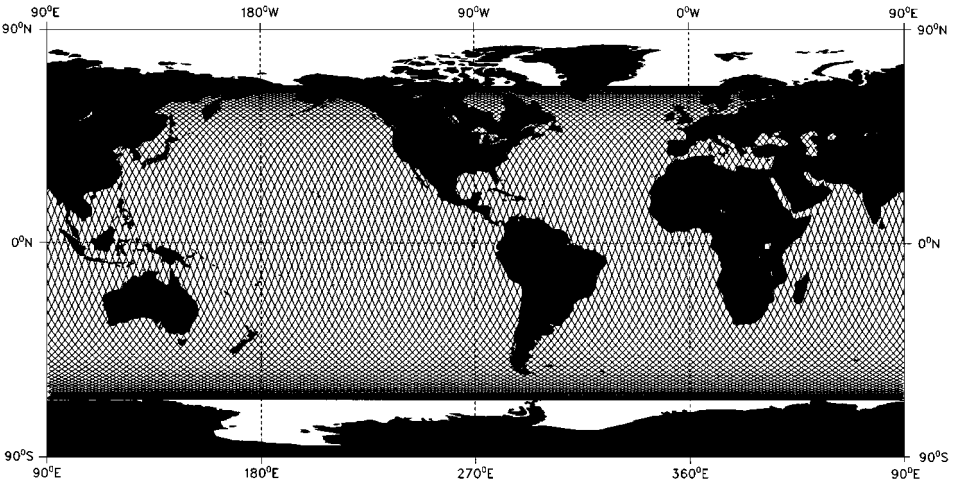

Figure 4 TOPEX/POSEIDON ground track over the ocean. This subsatellite pattern is repeated with 1-km lateral accuracy every 9.91859 days.

we are now in the era of multiple simultaneous altimetric missions. (At the time of writing, ERS-1 is dormant, in orbit.)

The TOPEX/POSEIDON Configuration

The August 1992 launch of the TOPEX/POSEIDON spacecraft was into an orbit with an altitude of about 1300 km and a subsatellite ground track as depicted in Figure 4. This ground track pattern repeats nearly exactly every 9.9 days (usually called the 10-day repeat orbit). At the time of this writing, more than four years of data have been obtained, with another four years possible. Technical details of the spacecraft can be found in a paper by Fu et al (1994) and the references therein.

Before discussing the results, we list the major corrections required to obtain the existing 2- to 3-cm accuracy. At these levels, there are numerous effects contributing errors near 1 cm root mean square (rms) to the total budget, and a complete discussion is beyond our scope. Potential users should be aware that experts have labored to properly formulate the data handling, and their products are now widely available in processed form (e.g. corrected, gridded, averaged, etc) so that others are spared a large complicated job. But all serious data users must have a working knowledge of the system basics.

PRECISION ORBIT DETERMINATION The spacecraft is tracked by three different systems: laser ranging, a ground-beacon Doppler system called DORIS

(Doppler Orbitography and Radio positioning Integrated by Satellite; Nouel et al 1988), and the Global Positioning System (GPS), with the latter often degraded by military interference with the signals. Tapley et al (1994) and Smith et al (1996) described in detail how these tracking data are combined with orbit estimation equations and improvements in the knowledge of the gravity field. At the present time, the residual rms orbital error is estimated to be about 2 cm.

GRAVITY FIELD (GEOID) AND GEODETIC REFERENCE FRAMES The gravity field enters in the measurements in two ways: through the gravity perturbations affecting the spacecraft orbit and through the use of the reference surface N in Equation 8. A vigorous effort was made to greatly improve knowledge of the Earth's gravity field (Tapley et al 1996), culminating in the most recent gravitational potential estimate (see Figure 5) called the Earth Geopotential Model 96 (EGM96; Lemoine et al 1997). The geoid undulation derived from this model is complete to spherical harmonic degree 360, although the estimates of the latter degrees are very uncertain. Preliminary tests of the geoid against oceanic circulation and independent orbit estimates suggest that the EGM96 error bars may be somewhat optimistic. The comparatively high-altitude spacecraft orbit is affected primarily by the long wavelengths (low spherical harmonic degrees), and the gravity field error is now a small component of the orbit error. A

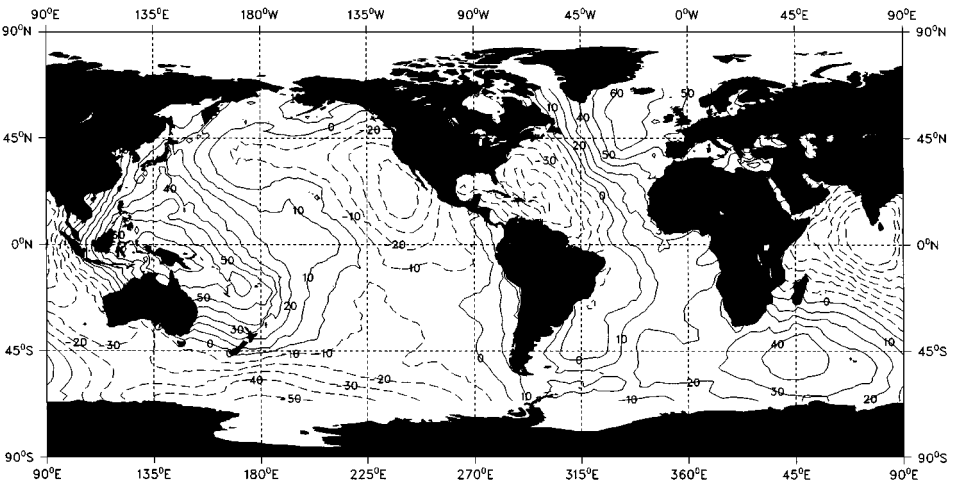

Figure 5 EGM96 geoid height, N, relative to an underlying reference spheroid (Lemoine et al 1997). Contours are in meters with a range from -105 to $+82$ m. Because $|\eta| \ll |N|$, the surface S is visually indistinguishable from N.

starting point for discussion of the high-accuracy geodetic reference frames for TOPEX/POSEIDON is Mueller's paper (1989).

ATMOSPHERIC WATER VAPOR Because tropospheric water-vapor content variability introduces spurious changes in apparent sea surface distance of up to 30 cm (Chelton 1988), the TOPEX/POSEIDON spacecraft carries a three-frequency microwave radiometer that provides a direct measure of atmospheric water vapor (see Ruf et al 1994, Stum 1994). The measurements are believed to be accurate to about 1 cm.

IONOSPHERE Variations in ionospheric free-electron content can produce spurious sea level variations of tens of centimeters. The dual frequency TOPEX altimeter measures the free-electron population, leading to a correction with an accuracy at the 1-cm level (see Imel 1994, Zlotnicki 1994).

TIDES Oceanic tides exist at semi-diurnal and diurnal periods, with small contributions at two weeks, one month, six months, one year, etc, which together produce oceanic elevation changes on the order of 2–3 m. These are the largest components of sea surface variability other than extreme surface waves. With the 10-day basic sampling of the repeat orbit, a semi-diurnal tide masquerades as (or "aliases" to) periods near 60 days; it is essential to remove the tidal components to render visible the much smaller signals of the general circulation. But TOPEX/POSEIDON is itself a high-precision global tide gauge, and the deep ocean tides are now known, as a result of the mission, to accuracies at the 1-cm level in elevation at many tidal frequencies (see Andersen et al 1995 and Shum et al 1997). All previous open ocean tide models are obsolete, but the problem is not completely closed (see Ray & Mitchum 1996 and below).

Although usually treated as an oceanic phenomenon distinct from the general circulation, tidal dissipation may play a major, conceivably dominant, role in mixing the ocean and hence in determining the strength of the so-called thermohaline circulation, which is so important to climate. With the high-accuracy models now available from TOPEX/POSEIDON, it has finally become possible to quantify and regionalize tidal dissipation, but the subject is rapidly changing—see, for example, Lyard & Le Provost (1997), or Munk (1998).

SURFACE EFFECTS (SEA-STATE BIAS AND OTHERS) The "footprint" or diameter of the radar pulse at the sea surface is about 7 km in moderate sea states. So-called electromagnetic (EM) bias effects arise from the failure of the returning radar pulse to show maximum energy corresponding to the position of the mean sea surface, as employed in large-scale dynamical equations (Chelton 1988). One effect arises because the power of back-scattered radiation is proportional to the local radius of curvature of long waves; typically, such waves have broad

flat troughs and narrow sharp peaks, and hence the radar return is stronger from the troughs. A second bias of the same sign occurs because the surface roughness created by wind reduces the back-scattered power, and the positions of these rough patches relative to crests and troughs depends in a complex way on the sea state and wind field (P Gaspar, personal communication).

Historically, the EM bias has usually been expressed as a fraction of the "significant wave height"—an archaic, but historically important, depiction of waves in terms of the average of the highest third of the waves present. [Phillips (1977, p. 188) discussed the relationship between significant wave height and more conventional statistical properties.] The bias values are around 1–2% of the significant wave height. However, the single parameter representation is known to be much too simple: The bias is dependent on the complete wave spectrum and not simply its total power. Thus, additional parameters have recently been introduced as polynomials in wave height and wind speed (Gaspar et al 1994, Rodriguez & Martin 1994, Chelton 1994), and there are strong dependences on EM wavelength (Walsh et al 1991, Stewart & Devalla 1994).

Another effect is associated with the non-Gaussian nature of the wave height distribution. Correcting the sea-state bias effect as a function of wave height assumes a symmetric wave height distribution. In practice, however, the skewed wave height distribution with a median shifted towards wave troughs introduces another bias in measured sea level, which is referred to as the skewness bias. Other surface effects are related to off-nadir antenna pointing angles and their effect on the estimate of wind speed and sea surface height. In regions of large amplitude surface waves, particularly at high southern latitudes, the sea-state bias effects may well be the largest error; much more work will be required to render the surface effects negligible at the 1-cm level.

ATMOSPHERIC LOAD Fluctuations in the weight of the over-lying atmosphere that manifest as surface pressure changes produce corresponding changes in the position of the sea surface. To the extent that the ocean responds statically, a local 1-millibar (mb) increase in atmospheric pressure depresses the sea surface by 1 cm. A uniform change in atmospheric pressure over the ocean does not move the sea surface; hence, measurements of atmospheric load must be made relative to the over-ocean average atmospheric pressure, which fluctuates by about 3 mb. The assumption of a static response ("isostatic" in geophysical jargon) is a surprisingly good one at all observable periods (e.g. Fu & Pihos 1994); Wunsch & Stammer (1997) review the subject. Regions where questions remain about the nature of the response include the tropics, where atmospheric pressure fluctuations are very small; semi-enclosed seas; and the western boundary current regions of all oceans. These areas are dynamically

distinct from the oceanic interior, but the signal-to-noise ratios are also poor there—and may well account for the apparent deviations from static response. Some uncertainty remains concerning the oceanic response at periods shorter than about 10 days, but the variance is small.

POLAR MOTION Wobble of the rotation axis of the Earth [including the 14-month free (Chandler) wobble and the forced annual component] introduces a time-dependent centrifugal term into the apparent gravity seen by any observer fixed to the surface of the Earth (Wahr 1988). With present accuracies, the equivalent sea level change of order 2 cm is significant, and thus polar motion is determined and included as a correction.

SAMPLING AND ALIASING The fundamental sampling interval for TOPEX/POSEIDON is 10 days—the return time to any fixed location. Classical sampling theory (e.g. Bracewell 1978) shows that time-dependent motions occurring at periods shorter than 20 days will alias to longer periods. As an example, the 12.42-h principal lunar tide, M_2, appears in a Fourier transform of the data at a fixed location with an apparent period of 62 days. The choice of TOPEX/POSEIDON orbit was in large measure dictated by the need to prevent aliasing of tidal frequencies into important lower frequencies such as zero (the time average) or the seasonal frequency—aliases that would have effectively precluded study of important oceanographic phenomena (see discussion by Parke et al 1987).

Oceanic variability occurs at all periods, from seconds to millions or billions of years. The extent of the occurrence of energetically significant aliasing of the periods shorter than 20 days into apparent low-frequency variability in the TOPEX/POSEIDON data is a complex issue because of the very great regional differences in the amplitudes and space/time scales of oceanic variability. Simple spatial filtering can much reduce the aliasing, and in common with many geophysical processes, the sea surface variability tends to have a "red" spectrum. For such a spectrum, the rapid decay of energy with frequency renders the measurements comparatively immune to aliasing, with the tides as a notable exception. The problem is exacerbated, however, by the dependence of the ocean circulation on the spatial derivatives of the elevation rather than on the elevation itself—as the frequency spectrum of sea surface slope is much less red than that for elevation. A full discussion is not yet available, but aspects are described by Salby (1982), Wunsch (1989), Chelton & Schlax (1994), and Greenslade et al (1997). Eventually, a more complete description will become necessary.

The ability to sample the ocean adequately to avoid significant temporal aliasing must be distinguished from the related but different ability to produce

uniformly accurate physical-space maps of sea surface topography. Generally speaking, by using spatial filtering, the 10-day repeat orbit of TOPEX/POSEIDON is adequate to reduce serious aliasing from high-frequency nontidal motions at the measurement positions. But because of the "diamond pattern" formed by the ground tracks in Figure 4, the sampling is inadequate for production of accurate maps of short spatial scales of elevation associated with eddies in the interiors of the diamonds (the short spatial scales, which are adequately sampled along track, cannot be extrapolated to the unsampled regions, but the long wavelengths can be usefully mapped). Temporal coverage does remain an issue in some regions of rapid change, such as near the meandering Gulf Stream (see Minster & Gennero 1995) and in some tropical regions. Should uniform high wavenumber mapping be required everywhere on the sea surface, then the only remedy is to fly additional altimeters; by good fortune, coverage may be adequate in the next few years to permit such mapping (Greenslade et al 1997).

THE TIME-VARIABLE CIRCULATION

Figure 6*a* shows the time-averaged sea surface from four years (October 12, 1992, to October 9, 1996) of TOPEX/POSEIDON data relative to the EGM96 geoid, spatially filtered to remove any oceanic spatial structures with wavelengths shorter than about 500 km. Such a surface contains any residual geoid errors, including errors in the spherical harmonic expansion coefficients, as well as errors of omission from coefficients simply set to zero (everything above spherical harmonic degree 360). Beginning with the earliest altimetric missions, it was recognized that the time-dependent ocean variability could be determined independently of errors in N. One either forms a time-mean $\overline{\eta}(\theta, \lambda)$, and works with anomalies $\Delta\eta = \eta - \overline{\eta}$ or, less commonly, with the discrete time-derivative $d\eta = [\eta(\theta, \lambda, t + \Delta t) - \eta(\theta, \lambda, t)]/\Delta t$. In either case, N no longer appears. (But at second order, errors in N affect the orbit determination and can introduce spurious time variability into the measurement.) The ease of this removal of geoid error has led to a large literature on the time variability of the ocean circulation as seen at the sea surface. Figure 6*b* shows, for example, the spatially smoothed anomaly in one 10-day period of the flow field relative to its four-year average.

Because of the novelty of the instrument, many papers have demonstrated by direct comparison with more conventional instruments that the measurements were accurate and believable. Thus, there are comparisons with, for example, tide gauges (Mitchum 1994), inverted echo sounders (Hallock et al 1995), current meters (Strub et al 1997, Wunsch 1997), atmospheric forcing climatologies (Chambers et al 1997, Stammer 1997b), and expendable temperature

measuring devices (XBTs; White & Tai 1995). There is no evidence for any inconsistency beyond known error estimates and sampling disparities between in situ and altimetric measurements of the variability on time scales between days and years. (Global mean sea level has been a troubling exception; see Nerem et al 1997.)

The current meter data, in particular, have been used (Wunsch 1997) to understand the vertical partitioning of the motions in the context of compensation in the vertical. Although the results are complicated in detail, and the coverage by current meters less than global, it appears that the sea level slope energy seen by the altimeter in low and middle latitudes is dominated by motions in which there is first-order movement (compensation) by the interior density field. Thus, qualitatively, the altimeter primarily reflects movement of the deep isopycnals (surfaces of constant density) and only secondarily that of motions extending unattenuated to the seafloor. High-latitude variability (poleward of about 40°) appears more barotropic (uncompensated) owing to the weaker stratification and large values of $|\phi|$ in Equation 6; very strong seasonal changes in the stratification also occur there.

Because of the dominant oceanographic paradigm of an unchanging general circulation, the novelty of being able to demonstrate oceanographic variability has produced a very large literature, too large to review here, that displays the degree of temporal variability in an immense variety of physical settings. *The greatest importance of TOPEX/POSEIDON has been its vivid demonstration that the ocean is a global-scale fluid constantly evolving on all time and space scales.* Special attention has been paid to high-energy regions such as the western boundary currents, the Antarctic Circumpolar Current, interior fronts, regions of strong topographic gradients, and the Mediterranean Sea, but for reasons of space, we omit specific discussion of the results.

The Annual Cycle

The seasonal cycle in the ocean is an important element in climate. Generally speaking, the oceanic response is the sum of a strong local effect (direct heat and moisture exchange with the atmosphere) plus a dynamical response from remote disturbances, believed to be primarily wind-related (Gill & Niiler 1973). TOPEX/POSEIDON measurements directly display the very large-scale thermal response (e.g. White & Tai 1995, Chambers et al 1997, Stammer 1997b) plus dramatic propagating structures. Figure 7 shows the amplitude and phase of the annual cycle of sea level. The very large amplitudes in the Kuroshio and Gulf Stream reflect the regions of intense wintertime air-sea exchange of heat there. Although the northern and southern hemispheres are approximately 180° out of phase, the ocean displays a complex spatial structure in its response to annual forcing. Among a host of features, note that the northern-hemisphere

ocean generally has a larger amplitude than the southern. It is apparent in the altimeter data that the annual cycle in the ocean shows very large variations from year to year and is not a simple periodic phenomenon.

Second Order Moments (Including Spectra and Rossby Wave Discussion)

Although the altimeter is extremely useful in regional studies, its great novelty is the ability to depict the global ocean. Several representations are required to fully understand the implications of the data. Let $\eta' = \eta - \langle \eta \rangle$, where the bracket denotes the four-year average elevation; then Figure 8*a* depicts the great spatial variability of $\langle \eta'^2 \rangle$, and Figure 8*b* that of the slope variance $(g/2\Omega)^2 \langle (\partial \eta'/\partial s)^2 \rangle$, with the bracket denoting a time average. The mean square of η' over four years is about 97 cm^2, for an rms variability of less than 10 cm—which makes clear the need for the elaborate error reduction procedure. The slope variance is related to the surface kinetic energy variance, K_E, through

$$K_E = \frac{g^2}{(2\Omega \sin \phi)^2} \left\langle \left(\frac{\partial \eta'}{\partial s} \right)^2 \right\rangle. \tag{9}$$

Equation 9 represents the component of kinetic energy from the cross-track geostrophic velocity multiplied by 2 under the assumption of local isotropy (Stammer 1997a). These variances can be broken up into their contributions by frequency band and (approximately only) by wavenumber band (Wunsch & Stammer 1995).

Figure 10 depicts the complex way in which the kinetic energy, as computed in Equation 9, shows an annual variability. These results display a spatial intricacy (e.g. in the high-latitude North Atlantic and the tropics) for which only the smallest beginnings of an explanation have as yet been attempted (White & Heywood 1995, Stammer & Böning 1996).

FREQUENCY/WAVENUMBER DEPICTION In view of the strong spatial inhomogeneities visible in Figures 7–9, as well as the complex geometry of the ocean boundaries, a conventional frequency/wavenumber representation of the global oceanic low-frequency variability is not the complete description that it would be in a (Gaussian) spatially and temporally homogeneous field. Nonetheless, the description remains useful and important. Figure 10 displays the frequency/wavenumber power spectrum as computed by Wunsch & Stammer (1995), but now recomputed from four years of data rather than the two years available at that time. Until TOPEX/POSEIDON was flown, many of the space/time scales in these figures were simply unmeasurable by any known means. Apart from the quantitative description that is now available, a major conclusion drawn from Figure 10 and other estimates is that the ocean varies on all space

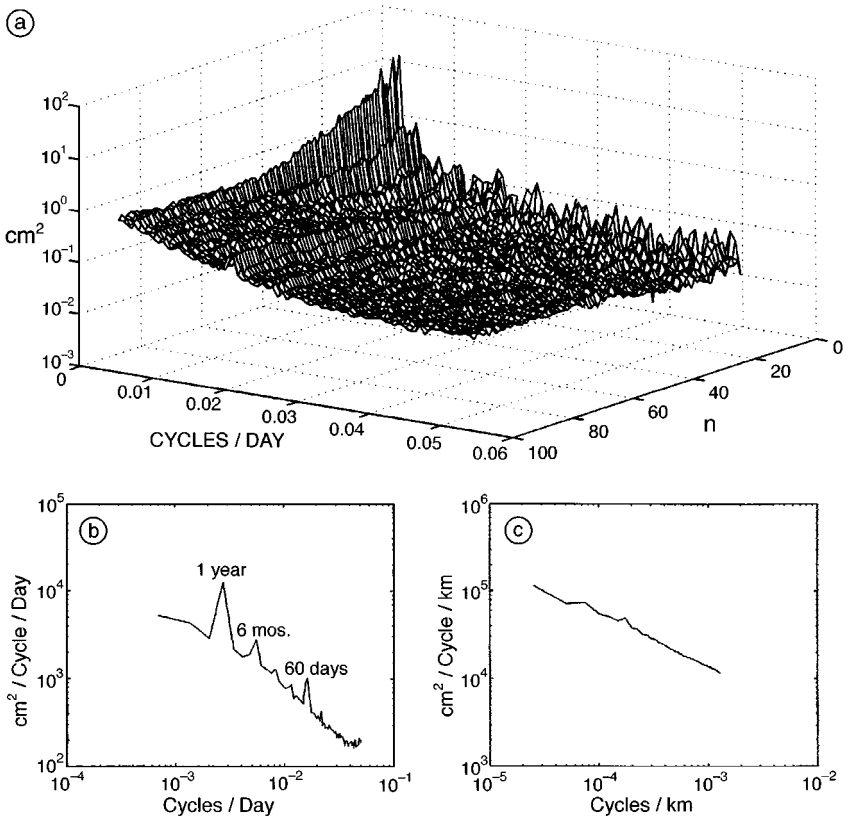

Figure 10 (*a*) Frequency/wavenumber energy spectrum computed from a spherical harmonic fit, as described by Wunsch & Stammer (1995), but from four years of data vs two. Wavenumbers are actually in terms of spherical harmonic order *n*, for which the wavelengths are approximately 40,000 km/*n*. The total power integrates to 41 cm^2 and contains no energy on spatial scales shorter than about 400-km wavelength. The major low-frequency feature is the annual cycle, which is broadband in wavenumber space. A small ridge near 60-day period has an rms amplitude of about 0.9 cm and represents the residual uncorrected M_2 and S_2 semidiurnal tidal constituents, which alias to this period. Much of this small residual is the surface manifestation of internal tides and is not predictable. These unpredictable tidal elements may continue to require that future altimetric missions fly in TOPEX/POSEIDON-like orbits to prevent the temporal aliases that are a feature of the Sun-synchronous orbits used for cheaper missions. (*b*) Frequency power density spectrum obtained from *a* by summing over all spherical harmonics. The annual, semi-annual, and 60-day tidal alias peaks are conspicuous. Some of the semi-annual peak is probably residual aliasing of diurnal tides. (*c*) Wavenumber power density spectrum, computed from *a* by summing over all frequencies and then converting (Wunsch & Stammer 1995) to the along-track great circle wavenumber spectrum of an equivalent homogeneous, isotropic process. Some high wavenumbers have been omitted because of the spatial filtering implicit in producing *a*.

and time scales; there are no spectral gaps, and there is no reason to believe that any element of the circulation is strictly steady.

The Mesoscale

Oceanic kinetic energy (Figures 8*b*, 9) is dominated by the so-called mesoscale, which lies very roughly on spatial scales of 30–1000 km, with time scales of 10–150 days. (There is no generally agreed upon definition; the motions correspond dynamically to the atmospheric "synoptic scale"—the weather systems.) Reviews of this subject can be found in Wunsch (1981b), Robinson (1983), and Holloway (1986b).

To describe these motions, Stammer (1997a) has broken the global altimetric elevation spectrum into regional representations. The focus of that study was to relate the regional dependence of eddy characteristics to eddy dynamics. The eddy length scale as determined from along-track sea-surface height data is closely related to the internal Rossby radius of deformation (see Figure 11). The ocean shows a strong relationship between the size of eddies that are responsible for mixing and property transports with latitudes. The small eddy size in high latitudes imposes stringent demands on numerical simulation in terms of spatial resolution.

Using the observed eddy length scale to normalize the local wavenumber, it was further found that the transformed wavenumber spectra from most of the

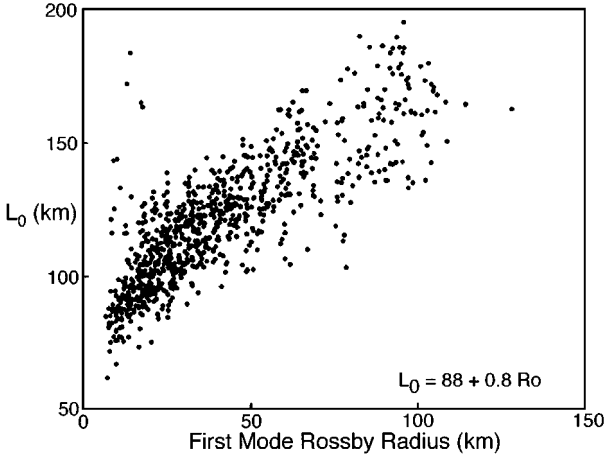

Figure 11 Scatter diagram of the eddy length scale L_0 estimated from the first zero-crossing of TOPEX/POSEIDON autocorrelation functions in 10° by 10° regions of the world ocean and plotted against the corresponding Rossby radii of the first baroclinic mode. The correlation coefficient between the fields is $r = 0.8$.

world ocean—upon normalization by the local variance—are consistent with each other in shape. An approximate universal rule for the energy distribution as a function of wavenumber can be written as

$$\begin{aligned}\Gamma_0(\tilde{k}) = 135\tilde{k}^{-0.7},\ 0.18 \le \tilde{k} \le 1.006,\\ 135\tilde{k}^{-2.8},\ 1.006 \le \tilde{k} \le 2.057,\\ 501\tilde{k}^{-4.6},\ 2.057 \le \tilde{k} \le 4.54.\end{aligned} \tag{10}$$

Here $\tilde{k} = k/k_0$, where k_0 is the wavenumber of the dominant local eddy scale. Other representations are possible too (Wunsch & Stammer 1995, Stammer 1997a). Although the power laws in Equation 10 bear an intriguing resemblance to the ones predicted by theories of geostraphic turbulance, there remain major theoretical issues in understanding the dynamical significance of these descriptions in terms of wave and turbulent interactions.

Rossby Wave Contributions

The theoretical linear response of the ocean to atmospheric forcing at the periods we are discussing is primarily in terms of so-called Rossby and topographic Rossby waves plus the Kelvin wave, which is boundary or equatorially trapped. In idealized form, the waves exist as both "barotropic" (extending to the seafloor unchanged) and "baroclinic" (compensated at a fixed intermediate depth; see Gill 1982). Because these waves have important dynamical consequences, and are a complete set for spectral representation, there have been a number of attempts to demonstrate their existence in altimetric variability. Because of the completeness, the waves can represent arbitrary motions, whether linear or not, in a topographically complex ocean with mean flows, and consequently the representation is of interest only if a very small number of waves can accurately describe the ocean over large geographical areas. That is, one seeks to understand the extent to which expressions like Equation 10 are composed primarily of linear wave-like phenomena or nonlinear "turbulent" ones. A linear ocean is much easier to understand than a nonlinear one, and hence the dynamical distinction is important.

Attempts to find barotropic elements have tended to be inconclusive at best (Fu & Davidson 1995, Chechelnitsky 1996), except at high latitudes (see Fu & Smith 1996), presumably because barotropic modes in the altimeter record are masked by the near-surface amplification of the baroclinic ones (Wunsch 1997). Baroclinic motions have fast phase and group velocities in the tropics relative to mid-latitudes, which permits use in these regions of comparatively short records. Convincing demonstrations of important linear baroclinic wave response in the tropics have been provided by Boulanger & Menkes (1995), Boulanger & Fu (1996), and Jacobs et al (1994).

Chelton & Schlax (1996; see also Polito & Cornillon 1997) described the appearance of baroclinic Rossby waves at mid-latitudes in a band of frequencies around one half to two cycles per year. Cipollini et al (1997) show that in the mid-latitude North Atlantic, the waves are strongly correlated with surface temperature anomalies. The most striking aspect of these results is that the waves appear to have phase speeds systematically higher (up to a factor of two) than produced by the theory for linear free waves. Understanding whether this anomaly is of dynamical significance, or whether it is a kinematic confusion of group and phase velocities in the presence of boundary reflections, forcing, and dissipation, is the subject of much current work (e.g. Killworth et al 1997, Qiu et al 1997). A quantitative estimate is not yet available of the fraction of the variability energy explicable by purely linear modes.

Jacobs & Mitchell (1996) have called attention to apparent low-frequency wave-like phenomena in the Southern Ocean [and described from non-altimetric data by White & Peterson (1996)], proposing a coupling with the geographically remote El Niño–Southern Oscillation in the ocean and atmosphere. The evidence, while suggestive, is based on records scarcely longer than one cycle of the supposed phenomenon and is dependent upon the GEOSAT measurements for an extended record.

Eddy Fluxes

An intense mesoscale eddy field in the ocean exists in mid-latitudes at periods much too short to be described by linear baroclinic waves. The implied nonlinearities show the possibility of significant eddy transports of momentum, heat, oxygen, and other chemical species. Before the advent of the altimeter data, the only way to determine the importance of eddy properties was through the long, laborious, and expensive deployment of moored instruments at specific positions in the ocean or through use of the erratic coverage by free drifters. Most of the available estimates of eddy momentum flux from altimetry are still from the GEOSAT instrument (e.g. Wilkin & Morrow 1994), although Strub et al (1997) used TOPEX/POSEIDON data; these studies support suggestions that near major meandering current systems, such as the Gulf Stream and Antarctic Circumpolar Current, eddy momentum fluxes are very important.

Theories that relate eddy transport properties (temperature, salt) to the thermodynamic mean state of a fluid were pioneered by Green (1970) for atmospheric conditions. These ideas, which are based on baroclinic instability mechanisms, have now been applied to the ocean (Visbeck et al 1997). Simultaneously, the theory of geostrophic turbulence was extended to provide estimates of eddy transports of a tracer field, with the eddy transport parameterized in terms of the mean flow field (Holloway 1986a, Held & Larichev 1996). Stammer (1997c) recently used these ideas and the eddy scales calculated from

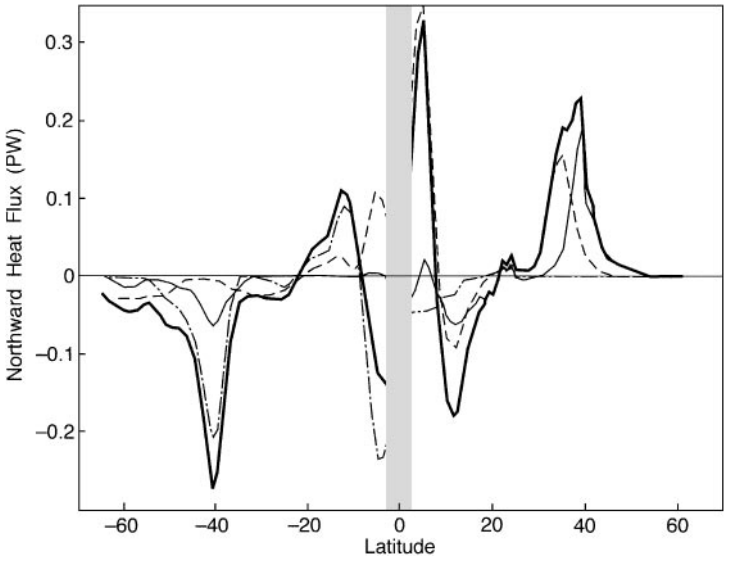

Figure 12 Zonally integrated meridional eddy transports of heat as estimated from TOPEX/POSEIDON eddy statistics. *Lines* represent a global integral (*bold solid*), the Atlantic Ocean (*thin solid*), the Pacific Ocean (*dashed*), and the Indian Ocean (*dash-dotted*). Estimates are not obtained in the *shaded low-latitude area*.

TOPEX/POSEIDON data to estimate the poleward eddy heat and salt transport for individual ocean basins (Figure 12). Results are consistent with the few available estimates from in situ data. Calculated eddy heat fluxes are small compared to the maximum heat transport by the ocean (Macdonald & Wunsch 1996), with the exception of low latitudes and near 40°N, a result that supports the importance of the eddy transports in the tropics and near western boundary currents.

Time Variation in Models

COMPARISONS WITH DATA The advent of altimetry made it possible for the first time to compare general circulation models (GCMs) globally to a uniform, time-evolving data set. These comparisons simultaneously produce insight into the models' shortcomings and provide an estimate of the relative error budgets of the models and observations. A major goal has been ultimately to combine the models with the altimetric observations in a physically and statistically reasonable way (called "fusion," "assimilation," or "estimation theory"). Detailed comparisons of model results and data are a necessary preliminary to such a step. Many regional comparisons are now available, and there are a few global ones (Fu & Smith 1996, Stammer et al 1996, Rapp et al 1996). Empirical orthogonal

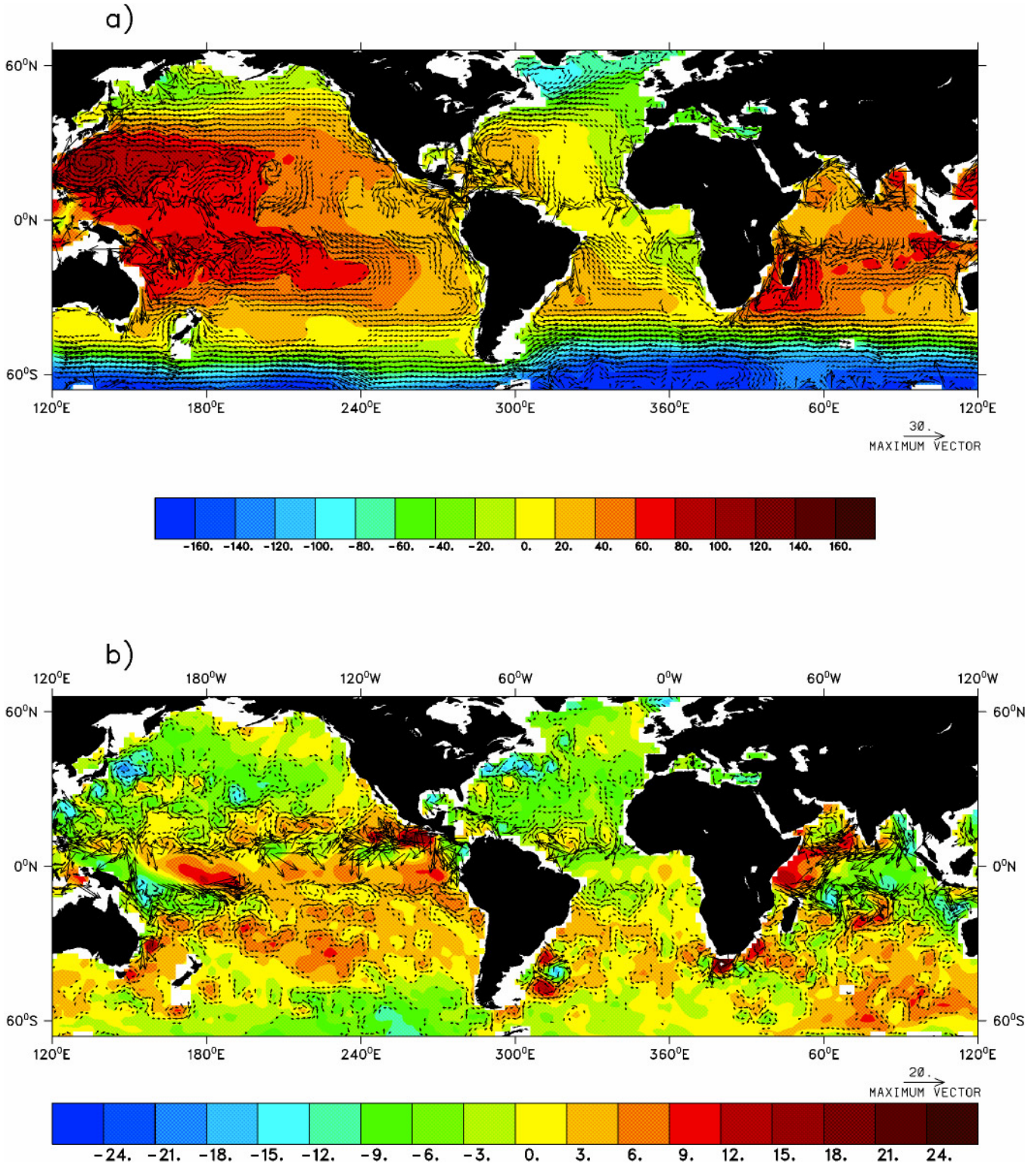

Figure 6

Figure 6 (*a*) Four-year average of the oceanic surface elevation, $\langle\eta\rangle = S - N$, from TOPEX/POSEIDON data. Superimposed are the geostrophically computed velocity vectors implied by Equations 2 and 3; the near-equatorial and small values are omitted for clarity. Note that all structures with a spatial wavelength smaller than 500 km have been omitted because they would be dominated by geoid error. (*b*) Example of the anomaly of elevation $\eta' = \eta - \langle\eta\rangle$, relative to time mean $\langle\eta\rangle$ in (*a*) during one 10-day period (March 10–20, 1993). The geostrophic flow vectors corresponding to the elevation anomaly are superposed. Wavelengths shorter than about 500 km have again been omitted to permit some visual clarity. The actual anomaly field is far more complex and visually dominated by the omitted small scales.

Figure 7 Amplitude (*a*) and phase (*b*) of the annual cycle of elevation in TOPEX/POSEIDON from four years of data. Amplitude is in centimeters, phase in degrees measured from January 1, 1993. Areas of extreme air/sea exchange produce large elevation changes as heat is added and removed by the atmosphere. The structures apparent in the quieter oceanic interior are related to wave-like motions. Note rough north/south phase shift by 180°; the detailed structure in the phases particularly in the tropics and at high latitudes is apparent.

(*Next page*)

Figure 8 (*a*) Root mean square (rms) elevation anomaly $\langle\eta\rangle$ and (*b*) $g^2/(\Omega)^2\langle(\partial\eta'/\partial s)^2\rangle = (\sin\phi)^2 \bullet$KE from four years of data. Units are in centimeters and $(\text{cm/s})^2$, respectively. The weighted kinetic energy is employed to avoid the equatorial singularity in the geostrophic kinetic energy. The very great inhomogeneity in oceanic variability with space is apparent here, with the quietest areas showing variability of less than 2 cm in elevation—close to the present noise level of the overall system.

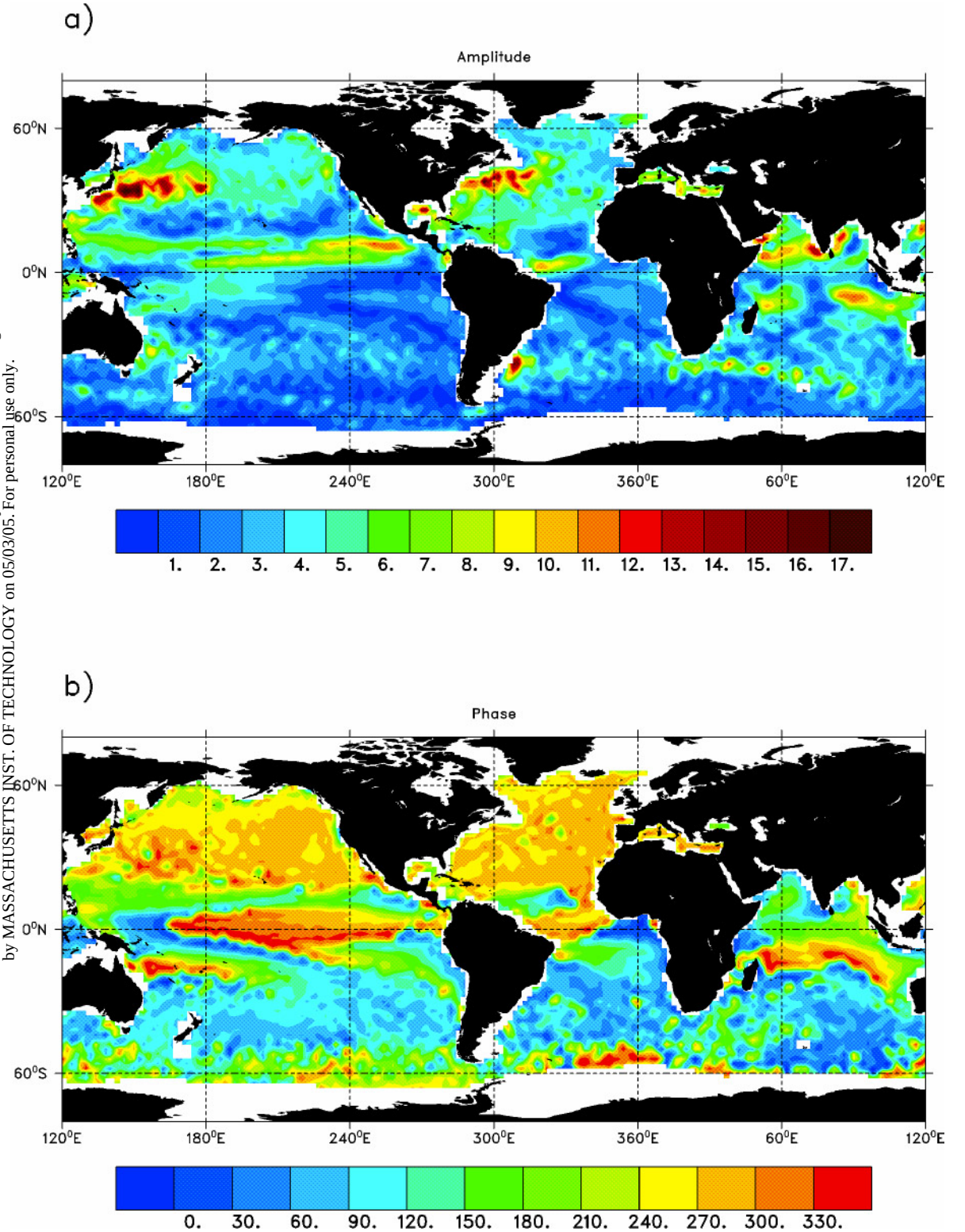

Figure 7

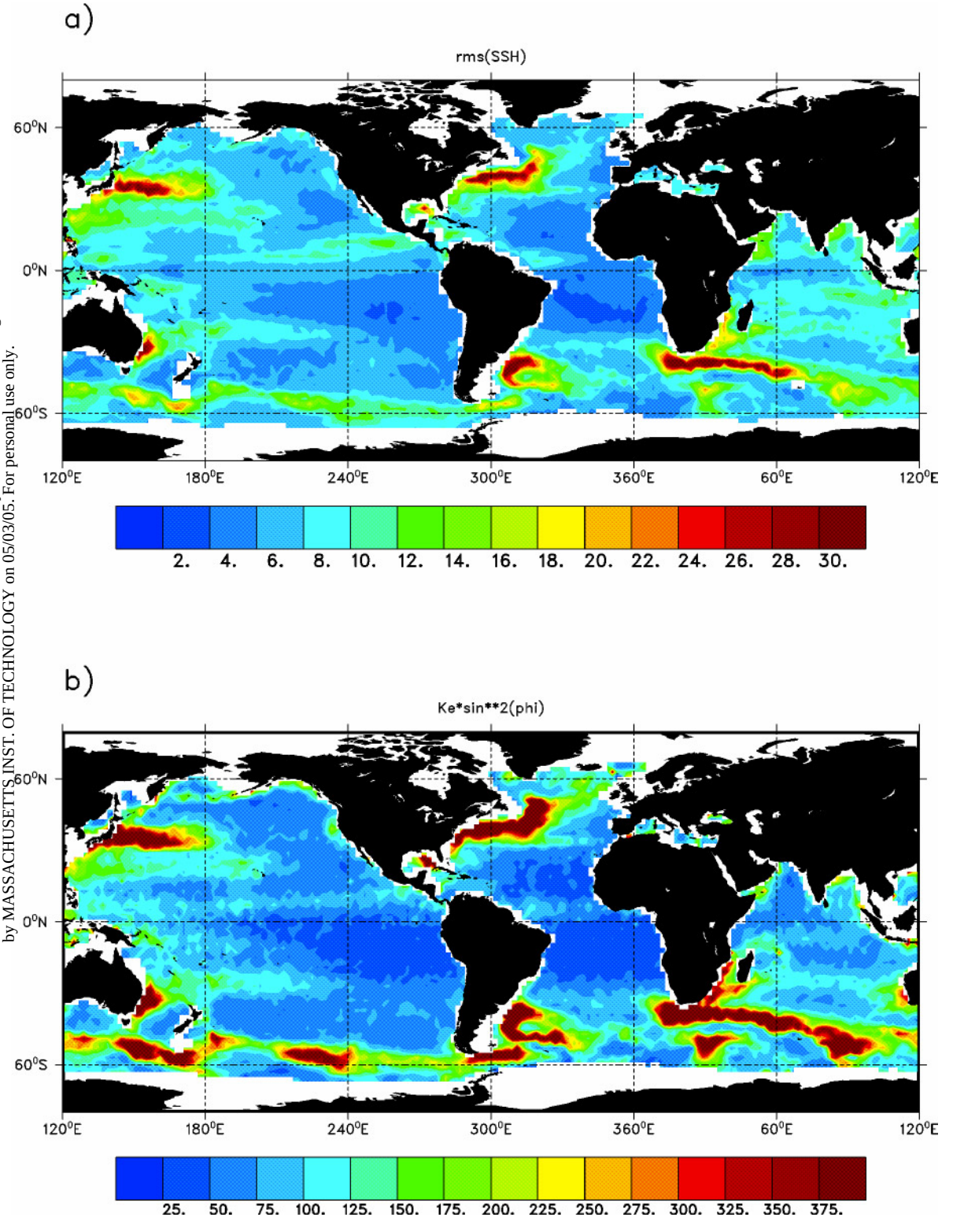

Figure 8

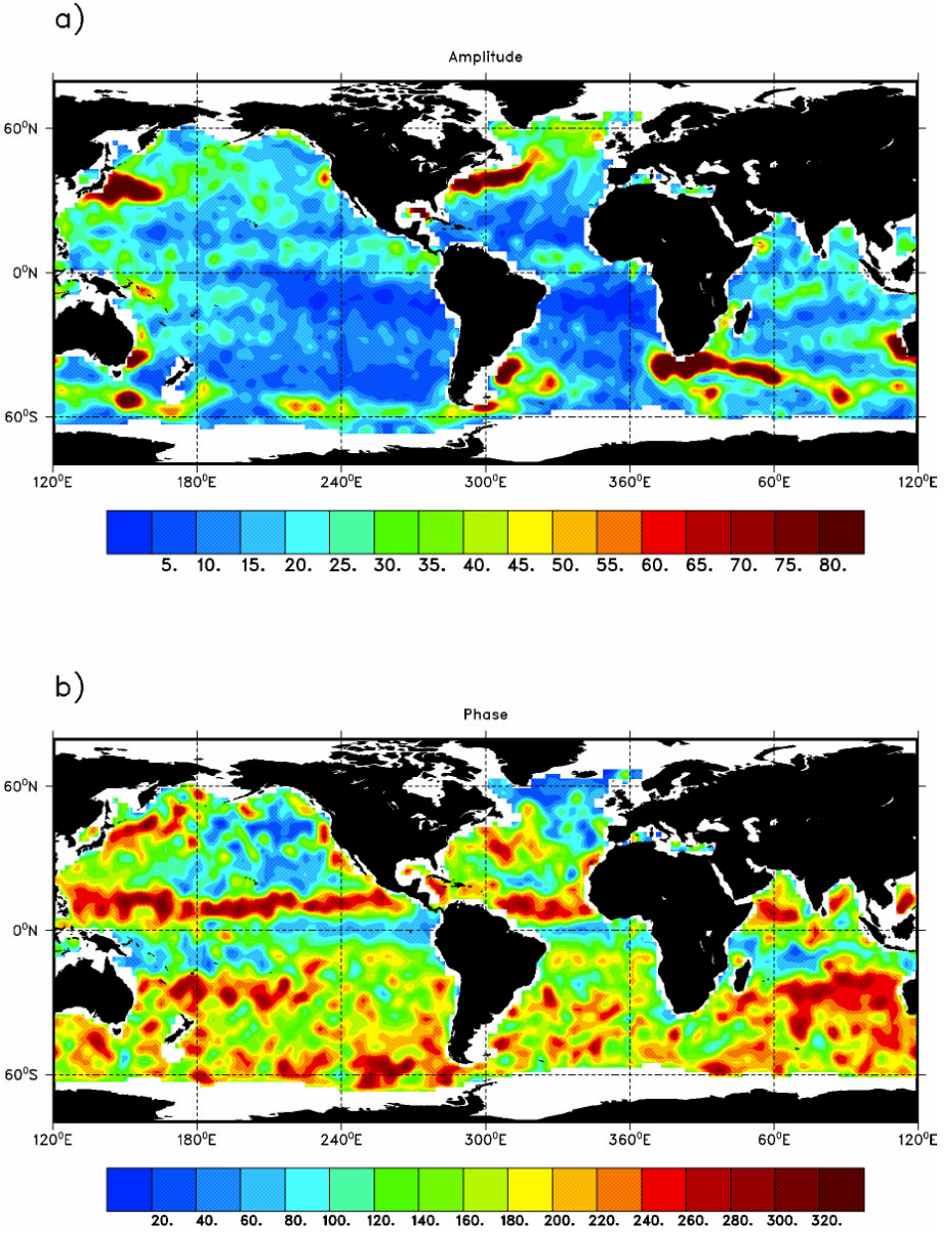

Figure 9 Amplitude and phase of $(\sin \phi)^2 \bullet$ KE at the annual period. These complex patterns are believed to be related to the ratios of direct forcing energies to the energy released in baroclinically and barotropically unstable regions of ocean circulation.

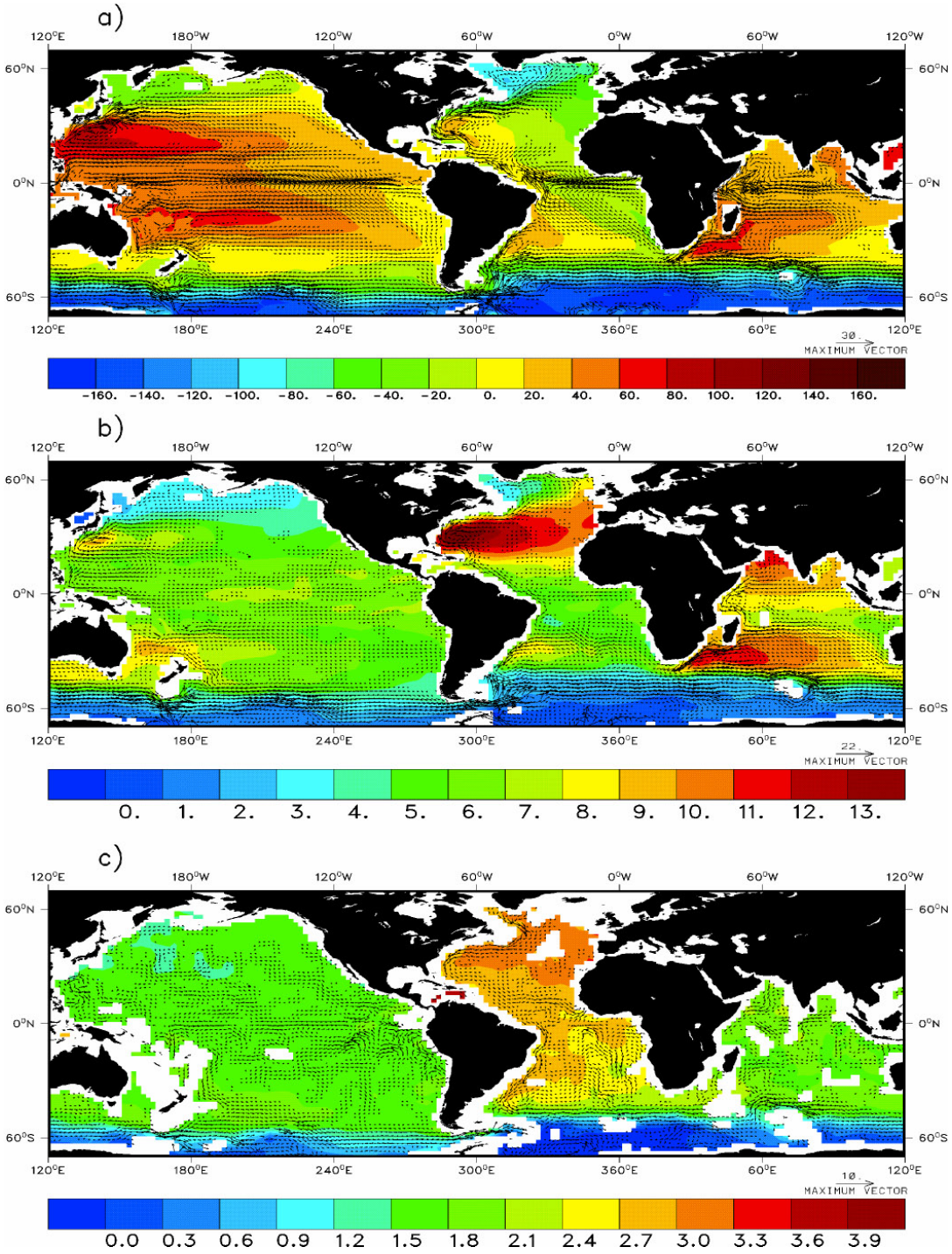

Figure 14

Figure 14 Results from a global optimization of a GCM, surface forcing fields, and a year of TOPEX/POSEIDON data (from Stammer et al 1997). (*a*) Time–mean velocity estimate $\tilde{\mathbf{v}}$ (cm/s) at 60-m depth, and the surface elevation $\tilde{\eta}$ in centimeters. (*b*) Potential temperature $\tilde{\theta}$ (in degrees Centigrade) and flow vectors in centimeters per second (small flow vectors are omitted) at level 10 (610 m in the model). (*c*) Same as *b*, except at 2450 m (level 15).

Figure 15 Changes required in the US National Center for Environmental Prediction (NCEP)-provided estimates in (*a*) the 10-day averaged freshwater flux field and (*b*) the heat flux as they emerge from the optimization for TOPEX/POSEIDON repeat cycle 21 (early September 1993). Contour intervals in *a* and *b* are 1 cm/year and 2 W m^{-2}, respectively. These changes are acceptable within plausible guessed errors for the NCEP product and are required for consistency with the oceanographic measurements used to produce the results in Figure 14.

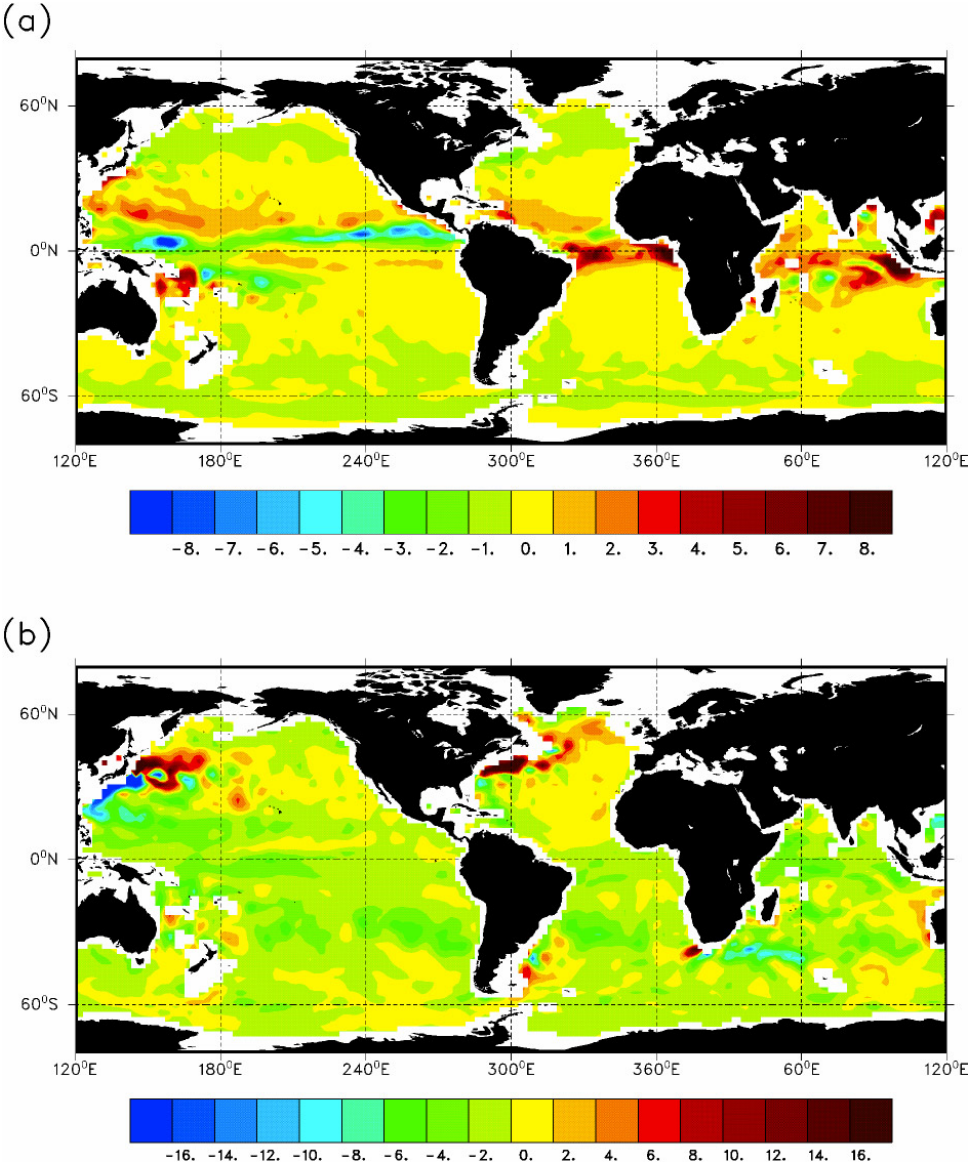

Figure 14

functions (EOFs), spectra, and spatial variability have all been used as descriptive tools. A summary would be that, even in the highest resolution models so far, there are both quantitative and qualitative disparities, manifested primarily as a failure of the models to display adequate variability on any time or length scale. We suspect, but cannot prove, that the low energies are largely a result of a failure to achieve adequate spatial resolution, which is probably less than 5 km at mid-latitudes, and to reduce the associated numerical friction. If the observed low-frequency/low-wavenumber variability is the result of scale coupling in the fluid, either kinematic or dynamic (turbulent cascades), coarse resolution models without observational constraints will systematically underpredict oceanic variability on all scales and, in particular, will underestimate eddy transports.

COMBINING DATA WITH MODELS: THE ESTIMATION PROBLEM Numerical models can be regarded as a summary of our imperfect knowledge of the ocean circulation as reflected in the equations of motion and the known boundary and initial conditions. Observations are another repository of information about the circulation: information that is incomplete and noisy in different ways from models. The estimation problem seeks to combine the two types of information into a single best-estimate of the ocean circulation.

A great deal is known of the generic model/data problem, and entire textbooks (Bennett 1992, Wunsch 1996) as well as hundreds of papers and meeting reports (e.g. Malanotte-Rizzoli 1996) exist on the problem in oceanography alone, not to speak of the immense general literature on estimation theory. As described by Wunsch (1996), in numerical practice, most systematic approaches to the problem reduce to the equivalent of a least-squares analysis minimizing the mean-square difference of the model output and the observations, suitably weighted by the error covariance matrices of the data and of the model. Adjustable or determinable parameters include the surface forcing (wind-stress and buoyancy fluxes), initial conditions, and model parameters such as friction coefficients. In nonglobal models, inflows through open sidewalls can be included as control parameters. Several different algorithms have been employed for numerical minimization. Many of these algorithms fall into the general classifications of sequential (filters and smoothers), iterative (adjoint or Pontryagin Principle), and Monte Carlo, and all have their adherents; the reader is referred to the literature for details. Here we will state only that the major practical difficulties can be understood as (*a*) the very large problem dimension for global scale estimation, (*b*) model nonlinearity, and (*c*) inability to properly specify model error covariances.

Most efforts have been devoted to regional scales, using simple ad hoc schemes with a focus on mapping the oceanic mesoscale. In these studies, the question of the correct weighting of model and data is ignored, and the model

is "nudged" toward the data through weights chosen subjectively or from simplified physical assumptions. Recently, more generally useful methods have come into use [e.g. Morrow & De Mey (1995), who use a Lagrange multiplier formulation (adjoint method) of least-squares]. For adequate mapping of the mesoscale by altimetry, multiple simultaneous missions are required; although this confluence of missions may soon occur, mesoscale mapping at the present time represents an extreme use of the data, and we do not pursue it here.

A demonstration of a systematic approach to the basin-scale problem was described by Stammer & Wunsch (1996). A general circulation model was formally linearized by numerically perturbing it in a sequence of regions and depths; the resulting Green's functions were employed as a new linear model to represent the differences between the TOPEX/POSEIDON observations and the forecast of those observations by the nonlinear model. [Great advantages exist if linear estimation theory can be used rather than nonlinear methods. The apparent success of the linearization for many ocean circulation problems contrasts with the meteorological experience (e.g. Daley 1991).] The estimation problem was then solved in terms of perturbations to the initial and boundary system conditions, with the full oceanic-state estimate as the original GCM values plus the linearized estimation values. A similar, but more elaborate, calculation also using tomographic data was carried out by Menemenlis et al (1997) for the Mediterranean Sea and by the Acoustic Thermometry of Ocean Climate (ATOC) Consortium (paper in preparation) for the entire North Pacific Ocean. This subject is in its infancy, but it is rapidly emerging as a major branch of ocean circulation studies and will likely dominate the observational discussion in the future.

THE ABSOLUTE AND TIME-INDEPENDENT CIRCULATIONS

The absolute circulation is defined from the instantaneous values of velocity, temperature, salinity, and other state variables. The separation into time-average and temporal anomaly is often useful, but it can also be artificial and confusing for several reasons. Because the spectra displayed above show no evidence for any low-frequency cut-off in oceanic variability, the time-averaged value can be an accident of the averaging interval. Furthermore, because the ocean circulation is a fluid flow governed by a nonlinear vector field theory, one cannot separate the dynamics into distinct time-dependent and time-independent components; the time-dependent flow generates mean or rectified flows, which are part of the time average. For this reason, it is better to speak of the absolute circulation at a fixed time t, whose average might be calculated and interpreted. Employing altimetry in this way requires an accurate geoid.

The Geoid Problem

The spatial variations in N relative to the reference ellipsoid E approach 100 m. $\tilde{N}(0)$ is any geoid (height) estimate made wholly independent of altimetry. Such geoids—deduced from spacecraft tracking, marine and land gravity measurements, etc—have errors exceeding 10 m. The magnitude of η is no more than 1 or 2 m; thus, $\tilde{N}(1) \equiv \langle S \rangle$ is an improved geoid. The approximation is adequate for many geophysical and military purposes and was used to justify the launch of GEOSAT.

Any information about the ocean circulation leads to an estimate of $\bar{\eta}$ and a further improved estimate of

$$\tilde{N}(2) = \tilde{N}(1) - \bar{\eta}. \tag{11}$$

Thus, there is a long and continuing symbiosis between altimetric measurements of circulation and the problems of depicting and understanding the Earth's gravity field. This relationship is of ever-growing importance, as efforts are underway to radically improve estimates of the marine geoid through dedicated spacecraft (e.g. Ganachaud et al 1997 and the references therein). In some regional studies (e.g. Porter et al 1996), the geoid height estimate $\tilde{N}(2)$ has been labeled a "synthetic" geoid. The terminology is misleading, as such an estimate is no more synthetic than any other. [Because there are correlations of bottom topography with the geoid (e.g. Watts et al 1985), high spatial resolution altimetry can be used to reconstruct much of the seafloor structure; see Hwang & Parsons (1995) for an example. In principle, the process could be reversed so that knowledge of the seafloor topography and of the underlying tectonics would be used to construct an accurate geoid. This procedure does not seem to have been pursued systematically, however, and in general, because of altimetric measurements, the geoid is now better known than the seafloor topography over much of the oceans.]

The computation in Equation 11 does not help the physical oceanographer. Despite the progress made in the past 20 years in geoid estimation, we must return to the problem described by Wunsch & Gaposchkin (1980): whether the independent information available in $\tilde{N}(0)$, $\tilde{S}$, and $\tilde{\eta}$ can be used to simultaneously estimate all three fields—thus improving knowledge of the absolute ocean circulation and of the geoid. [The interaction of physical oceanography and geodesy has a long and not always illuminating history—see Sturges (1974), Balazs & Douglas (1979).]

The initial point of departure for a discussion of the marine geoid thus has to be an analysis of the existing accuracy with which the oceanic general circulation is understood and its manifestation as a sea surface slope. This discussion is in turn best divided into results dependent upon conventional oceanographic analyses and those derived from GCMs.

Absolute Elevation from In Situ Oceanography

Any estimate of the oceanic flow on large scales, no matter how it is obtained, implies an absolute elevation $\tilde{\eta}$, and this elevation in turn, through Equation 11 implies a geoid estimate. A number of estimates of $\tilde{\eta}$ have been made on a global basis. Most of these (e.g. Stommel 1964, Levitus 1982) have employed global climatological averages of oceanic temperatures and salinities. These measurements are converted to a crude time-averaged density estimate $\langle \rho(\theta, \lambda, z) \rangle$, using an equation of state for seawater. The weight per unit area, written as the hydrostatic pressure of the fluid column, is then

$$p(\theta, \lambda, z) = \int_z^0 g \langle \rho(\theta, \lambda, z') \rangle dz' + p_s(\theta, \lambda) . \tag{12}$$

Here $p_s(\theta, \lambda)$ is the pressure, owing to the physical surface elevation

$$p_s(\theta, \lambda) = g \langle \rho(0)\, \eta(\theta, \lambda, t) \rangle. \tag{13}$$

The resulting pressure is then assumed to be uniform (that is, it is fully compensated) at some depth $z = z_c$, most often taken to be deep (below 1500 m or so) and constant with position. This assumption has two consequences: It fixes p_s and hence produces an estimate of $\langle \eta \rangle$, which we denote as $\tilde{\eta}_\rho$, and it implies that there is no horizontal flow at depth z_c. Thus, the latter is often labeled a "level-of-no-motion." An improved geoid is obtained from Equation 11 (see Figure 2). Wunsch (1981a) suggested that such calculations already had an accuracy of 10–25 cm. These remaining errors arise from three problems: The flow field implied by the level-of-no-motion assumption is not physically acceptable, as it fails to conserve mass and violates other physical laws (in other words, there is no evidence that the ocean has a simple compensation depth); the time-averaged hydrography is very inaccurate over much of the globe; and in many regions, the time-dependent flows can, through nonlinearities, contribute significantly to the time averages.

Macdonald (1995; see also Macdonald & Wunsch 1996) attempted to improve on these estimates by using temperature and salinity data to find a flow field satisfying the basic physical laws. She was able to make estimates of $\tilde{\eta}_\rho$ along various zonal and meridional lines in the global ocean; Figure 13 shows a comparison of some of her lines with those estimated from a recent geoid (JGM-3) and the altimetric estimate from Equation 8, as well as a pure numerical model estimate. The inconsistencies remain at the 10- to 25-cm level.

Ganachaud et al (1997) have further explored this problem, attempting to estimate quantitatively the impact on knowledge of the ocean circulation that would emerge from the flight of spacecraft dedicated to the direct determination

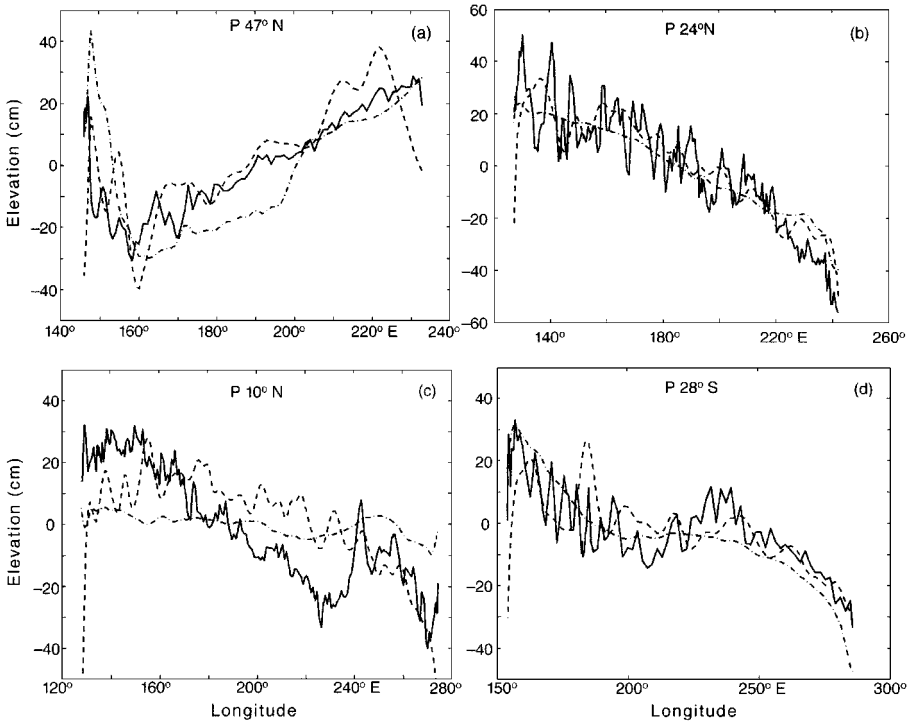

Figure 13 Comparison of η from TOPEX/POSEIDON data and the so-called JGM-3 geoid (Tapley et al 1997; *dashed lines*) with those from a hydrographic inversion (Macdonald 1995; *solid lines*), and with a global oceanic general circulation model (Stammer et al 1996; *dash-dot lines*) along several zonal lines in the Pacific Ocean (latitudes 47°N, 24°N, etc). Agreement is generally at the 10-cm level or better, but the discrepancies are oceanographically of first-order importance.

of N. The discussion is a complicated one, involving production of error covariance matrices for $\tilde{N}$ derived from hypothetical missions, as compared with those from estimates of $\tilde{\eta}_\rho$. A summary conclusion is that major improvements in the ocean circulation could be obtained if missions can meet very demanding design specifications.

Absolute Altimetry in Models

As with the temporal anomalies, the best use of altimetry is in combination with an accurate general circulation model. Conceptually, the use of absolute altimetry is identical to the temporal anomaly data: minimization of an objective function that represents the weighted mean square difference between the model output and the observations. If the absolute altimetry is to be employed with a

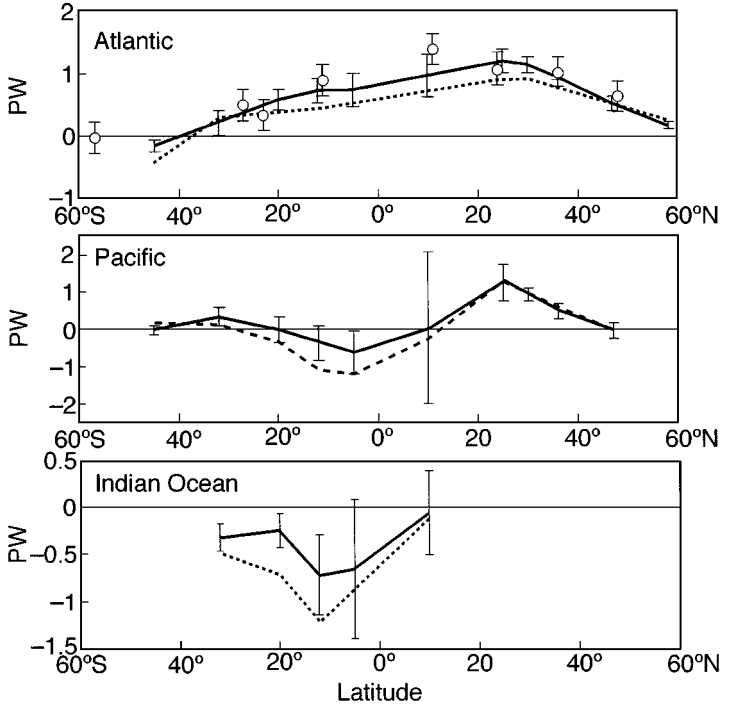

Figure 16 Meridional heat transport (in 10^{15} W) estimated from the last six months of the constrained (*solid lines*) and unconstrained model (*dashed lines*) for the Atlantic Ocean, the Pacific, and the Indian Ocean (from Stammer et al 1997). *Vertical bars* show the rms variability of the transports estimated over individual 10-day periods. *Open circles* and *bars* show similar estimates and their uncertainties obtained by Macdonald & Wunsch (1996).

model of the absolute circulation, terms are added to the objective function of the form $[\eta_{mod}(\theta_i, \lambda_i, t) - \eta_{alt}(\theta_i, \lambda_i, t)]^2$, where η_{mod} is the model representation of the sea surface elevation at position θ_i, λ_i at time t. Because η_{alt} contains any remaining geoid error, the weighting of these terms must properly account for that error; in turn, this means that the geographical spatial error covariance, R, is required for whatever geoid is being used. R is a square matrix of dimension equal to the number of horizontal grid points in the general circulation model; calculating and using it represents a major computational effort.

Recently it has become possible to carry out the minimization implied by the use of global absolute altimetry, using the values of R for the EGM96 geoid (M-C Kim, personal communication) and a global circulation model of Marshall et al (1997). The particular algorithm used was iterative and employed an adjoint to

the original model; the adjoint was generated using a special compiler (Giering & Kaminski 1997) that operates on the forward model code. Although thus far restricted by computer limitations to 2° of horizontal resolution (the number of model grid points is 180 by 80 horizontally by 21 vertically), it is possible to produce estimates of the ocean circulation on a 10-day basis in such a way that the model is consistent with the 10-day absolute surface topography, with time-varying surface topography and with the known meteorological forcing and basic temperature and salinity data for the ocean (Stammer et al 1997). Figure 14 depicts the time–mean absolute velocity at 60, 610, and 2450 m; the corresponding absolute surface elevation (Figure 14*a*); and the temperature field during the year 1995 from a combined model/data optimization (compare to Figure 6*a*). Figure 15 shows, as an example of what is now possible, the estimated adjustment to the air-sea freshwater flux (Figure 15*a*) and heat flux (Figure 15*b*) required to render the model consistent with the observations. Figure 16 shows how the TOPEX/POSEIDON data modify the model estimate of the climatologically important meridional flux of heat. Results from this form of model/data combination are not yet definitive, but they will become so over the next several years. The major issues are adequate computer power and the need to more clearly formulate expressions of model error; data errors also remain inadequately known.

THE FUTURE

TOPEX/POSEIDON altimetry has demonstrated the first practical global observation system for the oceanic general circulation. Remaining errors in the present system will gradually be reduced as understanding of the residual error sources improves. The combination of TOPEX/POSEIDON data with that from simultaneous missions of lower accuracy and precision (ERS-1 and 2 and GEOSAT-Follow-On) and more traditional in situ data will, over the next few years, provide a greatly improved estimate of oceanic variability on time scales from a few days to a decade. As oceanic GCMs continue to improve, there will be ever more accurate three-dimensional estimates of the absolute circulation on a frequent basis (perhaps weekly), with an emerging understanding on the limits of oceanic forecast skill.

These things can all be expected with a considerable degree of confidence because they are dependent primarily upon data now in hand. The real uncertainty concerns the future of high-accuracy altimetric missions. Spacecraft, because of their great expense and public visibility, are flown in a political arena whose wisdom is not easily predicted; furthermore, the vagaries of launch and on-board hardware and software failures render all such systems vulnerable to premature and catastrophic ends. At the present time, barring such failures,

satellite altimetry of the TOPEX/POSEIDON class appears assured for several years into the twenty-first century (current rubrics are Jason, ENVISAT, etc). As the data set grows, and our skill in interpreting it improves, we can anticipate that study of the ocean circulation will finally become a true quantitative science freed from the straitjacket of inadequate observation technology.

ACKNOWLEDGMENTS

P Gaspar, L-L Fu, D Chelton, and R Rapp provided many helpful comments. Supported in part by contracts from the National Aeronautics and Space Administration (NAG5-3724) and the Jet Propulsion Laboratory (958125).

Literature Cited

Andersen OB, Woodworth PL, Flather RA. 1995. Intercomparison of recent ocean tide models. *J. Geophys. Res.* 100:25261–82

Balazs EI, Douglas BC. 1979. Geodetic leveling and the sealevel slope along the California coast. *J. Geophys. Res.* 84:6195–6206

Bennett AF. 1992. *Inverse Methods in Physical Oceanography.* Cambridge: Cambridge Univ. Press. 346 pp.

Boulanger J-P, Fu L-L. 1996. Evidence of boundary reflection of Kelvin and first mode Rossby waves from TOPEX/POSEIDON sea level data. *J. Geophys. Res.* 101:16361–71

Boulanger J-P, Menkes C. 1995. Propagation and reflection of long equatorial waves in the Pacific Ocean during the 1992–1993 El Nino. *J. Geophys. Res.* 100:25041–60

Bracewell RN. 1978. *The Fourier Transform and Its Applications.* New York: McGraw-Hill. 444 pp.

Chambers DP, Tapley BD, Stewart RH. 1997. Long-period ocean heat storage rates and basin-scale heat fluxes from TOPEX. *J. Geophys. Res.* 102:10525–33

Chechelnitsky M. 1996. *Global barotropic variability of the ocean in response to atmospheric forcing based on multichannel regression and Kalman filter techniques.* MS thesis. Mass. Inst. Technol./Woods Hole Oceanogr. Inst. Joint Program. 112 pp.

Chelton DB. 1988. *WOCE/NASA Altimeter Algorithm Workshop. US WOCE Tech. Rep. 2.* US Planning Off. World Ocean Circ. Exp., Texas A & M Univ., College Station, Texas. 70 pp.

Chelton DB. 1995. The sea state bias in altimeter estimates of sea level from colinear analysis of TOPEX data. *J. Geophys. Res.* 99:24995–5008

Chelton DB, Schlax MG. 1994. The resolution capability of an irregularly sampled dataset: with application to Geosat altimeter data. *J. Atmos. Ocean Technol.* 11:534–50

Chelton DB, Schlax MG. 1996. Global observations of oceanic Rossby waves. *Science* 272:234–38

Cipollini P, Cromwell D, Jones MS, Quartly GD, Challenor PG. 1997. Concurrent altimeter and infrared observations of Rossby wave propagation near 34°N in the Northeast Atlantic. *Geophys. Res. Lett.* 24:885–92

Daley R. 1991. *Atmospheric Data Analysis.* Cambridge: Cambridge Univ. Press. 457 pp.

Dietrich G, Kalle K, Krauss W, Siedler G. 1975. *General Oceanography, An Introduction.* Transl. S Roll, HU Roll. New York: Wiley. 626 pp. 2nd ed. (From German)

Douglas BC, Cheney RE. 1990. Geosat: Beginning a new era in satellite oceanography. *J. Geophys. Res.* 95:2833–36

Douglas BC, McAdoo DC, Cheney RE. 1987. Oceanographic and geophysical applications of satellite altimetry. *Rev. Geophys. (Suppl. US Natl. Rep. Int. Union Geod. Geophys. 1983–1986)* 25:875–80

Fu L-L, Cheney RE. 1995. Application of satellite altimetry to ocean circulation studies: 1987–1994. *Rev. Geophys. (Suppl. US Natl. Rep. Int. Union Geod. Geophys., 1991–1994)* 32:213–23

Fu L-L, Christensen EJ, Yamarone CA, Lefebvre M, Ménard Y, et al. 1994. TOPEX/POSEIDON mission overview. *J. Geophys. Res.* 99:24369–82

Fu L-L, Davidson RA. 1995. A note on the barotropic response of sea level to time-dependent wind forcing. *J. Geophys. Res.* 100:24955–63

Fu L-L, Pihos G. 1994. Determining the response of sea level to atmospheric pressure using TOPEX/POSEIDON data. *J. Geophys. Res.* 99:24633–42

Fu L-L, Smith RD. 1996. Global ocean circulation from satellite altimetry and high-resolution computer simulation. *Bull. Am. Meteorol. Soc.* 77:2625–36

Ganachaud A, Wunsch C, Kim M-C, Tapley B. 1997. Combination of TOPEX/POSEIDON data with a hydrographic inversion for determination of the oceanic general circulation. *Geophys. J. Int.* 128:708–22

Giering R, Kaminski T. 1997. Recipes for adjoint code construction. *ACM Trans. Math. Software.* In press

Gaspar P, Ogor F, Le Traon P-Y, Zanife O-Z. 1994. Estimating the sea state bias of the TOPEX and POSEIDON altimeters from cross-over differences. *J. Geophys. Res.* 99:24981–94

Gill AE. 1982. *Atmosphere-Ocean Dynamics.* New York: Academic. 662 pp.

Gill AE, Niiler PP. 1973. The theory of the seasonal variability in the ocean. *Deep-Sea Res.* 20:141–77

Green JSA. 1970. Transfer properties of the large-scale eddies and the general circulation of the atmosphere. *Q. J. R. Meteorol. Soc.* 96:157–85

Greenslade DJM, Chelton DB, Schlax MG. 1997. The midlatitude resolution capability of sea level fields constructed from single and multiple satellite altimeter datasets. *J. Atmos. Ocean. Technol.* 14:849–70

Hallock ZR, Jacobs GA, Mitchell JL. 1995. Kuroshio sea surface height fluctuations observed simultaneously with inverted echo sounders. *J. Geophys. Res.* 100:24987–94

Heiskanen WA, Moritz H. 1967. *Physical Geodesy.* San Francisco: Freeman. 364 pp.

Held I, Larichev VD. 1996. A scaling theory for horizontally homogeneous, baroclinically unstable flow on a β-plane. *J. Atmos. Sci.* 53:946–52

Helland-Hansen B, Nansen F. 1920. Temperature variations in the North Atlantic Ocean and in the atmosphere. *Smithson. Misc. Collect.* 70(4). 408 pp.

Holloway G. 1986a. Estimation of oceanic eddy transports from satellite altimetry. *Nature* 323:243–44

Holloway G. 1986b. Eddies, waves, circulation and mixing: statistical geofluid mechanics. *Annu. Rev. Fluid Mech.* 18:91–147

Hwang C, Parsons B. 1995. Gravity anomaly determination from Seasat, Geosat, ERS-1 and TOPEX/ POSEIDON altimetry and ship gravity; a case study over the Reyjkanes Ridge. *Geophys. J. Int.* 122:551–68

Imel DA. 1994. Evaluation of the TOPEX/ POSEIDON dual-frequency ionosphere correction. *J. Geophys. Res.* 99:24895–906

Jacobs GA, Hurlburt HE, Kindle JC, Metzger EJ, Mitchell JL, et al. 1994. Decadal-scale trans-Pacific propagation and warming effects of an El Niño anomaly. *Nature* 370:360–63

Jacobs GA, Mitchell JL. 1996. Ocean circulation variability associated with the Antarctic circumpolar wave. *Geophys. Res. Lett.* 23:2947–50

Killworth P, Chelton DB, de Szoeke RA. 1997. The speed of observed and theoretical long extra-tropical planetary waves. *J. Phys. Oceanogr.* 27:1946–66

Lemoine F, Smith DE, Kunz L, Smith R, Pavlis EC, et al. 1997. The development of the NASA GSFC and NIMA Joint Geopotential Model. *Proc. Int. Symp. Gravity, Geoid and Marine Geodesy, IAG Symp.*, ed. H Fujimoto. Springer-Verlag. In press

Levitus S. 1982. *Climatological Atlas of the World Ocean. NOAA Prof. Pap. 13.* 173 pp. (plus microfiche)

Lyard FH, Le Provost C. 1997. Energy budget of the tidal hydrodynamics model FES94.1. *Geophys. Res. Lett.* 24:687–90

Macdonald AM. 1995. *Oceanic fluxes of mass, heat and freshwater: a global estimate and perspective.* PhD thesis. Mass. Inst. Technol./World Health Org. Int. 326 pp.

Macdonald A, Wunsch C. 1996. The global ocean circulation and heat flux. *Nature* 382: 436–39

Malanotte-Rizzoli P, ed. 1996. *Modern Approaches to Data Assimilation in Ocean Modeling*. Amsterdam: Elsevier. 455 pp.

Marshall J, Adcroft A, Hill C, Perelman L, Heisey C. 1997. A finite-volume, incompressible Navier Stokes model for studies of the ocean on parallel computers. *J. Geophys. Res.* 102:5753–66

McGoogan JT. 1975. Satellite altimetry applications. *IEEE Trans. Microwave Theory Technique.* MTT-23:970–78

Menemenlis D, Webb AT, Wunsch C, Send U, Hill C. 1997. Basin-scale ocean circulation from combined altimetric, tomographic and model data. *Nature* 385:618–21

Minster J-F, Gennero M-C. 1995. High frequency variability of western boundary currents using ERS 1 three-day repeat altimeter data. *J. Geophys. Res.* 100:22603–12

Mitchum GT. 1994. Comparison of TOPEX sea surface heights and tide gauge sea levels. *J. Geophys. Res.* 99:24541–54

Morrow R, De Mey P. 1995. Adjoint assimi-

lation of altimetric, surface drifter, and hydrographic data in a quasi-geostrophic model of the Azores Current. *J. Geophys. Res.* 100:25007–25

Mueller II. 1989. Reference coordinate systems: an update. In *Theory of Satellite Geodesy and Gravity Field Determination*, ed. F Sansò, R Rummel, *Lect. Notes Earth Sci.*, 25:153–93. Berlin: Springer-Verlag

Munk W. 1998. Once again, once again: tidal friction. *Prog. Oceanogr.* In press

Nerem RS, Haines BJ, Hendricks J, Minster JF, Mitchum GT, White WB. 1997. Improved determination of global mean sea level variations using TOPEX/POSEIDON altimeter data. *Geophys. Res. Lett.* 11:1331–34

Nouel F, Bardina J, Jayles C, Labrune Y, Truong B. 1988. DORIS: a precise satellite positioning Doppler system. In *Astrodynamics 1987, Adv. Astron. Sci.*, ed. JK Soldner, AK Misra, RE Lindberg, W Williamson, 65:311–20. Springfield, VA: Am. Astron. Soc.

Oriol-Pibernat E. 1990. The ERS-1 satellite: oceanography from space. In *Microwave Remote Sensing for Oceanographic and Marine Weather-Forecast Models*, ed. RA Vaughan, *NATO ASI Ser. C* 298:339–53. Dordrecht: Kluwer

Parke ME, Stewart RH, Farless DL, Cartwright DE. 1987. On the choice of orbits for an altimetric satellite to study ocean circulation and tides. *J. Geophys. Res.* 92:11693–707

Pedlosky J. 1987. *Geophysical Fluid Dynamics.* New York: Springer-Verlag. 710 pp. 2nd ed.

Phillips OM. 1977. *The Dynamics of the Upper Ocean.* Cambridge: Cambridge Univ. Press. 336 pp. 2nd ed.

Polito PS, Cornillon P. 1997. Long baroclinic Rossby waves detected by TOPEX/POSEIDON. *J. Geophys. Res.* 102:3215–36

Porter DL, Glenn SM, Dobson EB, Crowley MF. 1996. Extension and validation of a Gulf Stream GEOSAT synthetic geoid. *J. Atmos. Ocean. Technol.* 13:514–31

Qiu B, Miao W, Müller P. 1997. Propagation and decay of forced and free baroclinic Rossby waves in off-equatorial oceans. *J. Phys. Oceanogr.* In press

Rapp RH, Zhang C, Yi Y. 1996. Analysis of dynamic ocean topography using TOPEX data and orthonormal functions. *J. Geophys. Res.* 101:22583–98

Ray RD, Mitchum GT. 1996. Surface manifestation of internal tides generated near Hawaii. *Geophys. Res. Lett.* 23:2101–4

Robinson AR, ed. 1983. *Eddies in Marine Science.* Berlin: Springer-Verlag. 609 pp.

Rodriguez ER, Martin JM. 1994. Assessment of the TOPEX altimeter peformance using waveform retracking. *J. Geophys. Res.* 99:24971–80

Ruf CS, Keihm SJ, Subramanya B, Janssen MA. 1994. TOPEX/POSEIDON microwave radiometer performance and in-flight calibration. *J. Geophys. Res.* 99:24915–26

Rummel R, Sansò F, eds. 1993. *Satellite Altimetry in Geodesy and Oceanography. Lect. Notes Earth Sci. 50.* Berlin: Springer-Verlag. 479 pp.

Salby ML. 1982. Sampling theory for asynoptic satellite observations. Part 1. Space-time spectra, resolution and aliasing. *J. Atmos. Sci.* 39:2577–600

Shum C-K, Woodworth PL, Andersen OB, Egbert G, Francis O, et al. 1997. Accuracy assessment of recent ocean tide models. *J. Geophys. Res.* In press

Smith AJE, Visser PNAM, Ambrosius BAC, Wakker KF. 1996. TOPEX/Poseidon orbit error assessment. *J. Geod.* 70:546–53

Stammer D. 1997a. Global characteristics of ocean variability from regional TOPEX/POSEIDON altimeter measurements. *J. Phys. Ocean* 27:1743–69

Stammer D. 1997b. Steric and wind-induced changes in TOPEX/POSEIDON large-scale sea surface topography variations. *J. Geophys. Res.* 102:20987–1010

Stammer D. 1997c. On eddy characteristics, eddy transports and mean flow properties. *J. Phys. Ocean.* In press

Stammer D, Böning B. 1996. Generation and distribution of mesoscale eddies in the North Atlantic Ocean. In *The Warm Water Sphere of the North Atlantic Ocean*, ed. W Krauss, pp. 159–63. Berlin: Gebrüder Bornträger

Stammer D, Tokmakian R, Semtner A, Wunsch C. 1996. How well does a 1/4° global circulation model simulate large-scale oceanic observations? *J. Geophys. Res.* 101:25779–811

Stammer D, Wunsch C. 1996. The determination of the large-scale circulation of the Pacific Ocean from satellite altimetry using model Green's functions. *J. Geophys. Res.* 101:18409–32

Stammer D, Wunsch C, Giering R, Zhang QK, Marotzke J, et al. 1997. The global ocean circulation estimated from TOPEX/POSEIDON altimetry and a general circulation model. *Rep. No. 49 Cent. Global Change Sci.*, Mass. Inst. Technol. 40 pp.

Stewart RH. 1985. *Methods of Satellite Oceanography*. Berkeley: Univ. Calif. Press. 360 pp.

Stewart RH, Devalla B. 1994. Differential sea-state bias: a case study using TOPEX/POSEIDON data. *J. Geophys. Res.* 99:25009–14

Stommel H. 1964. Summary charts of the mean dynamic topography and current field at the surface of the ocean, and related functions of

the mean wind-stress. In *Studies on Oceanography Dedicated to Professor Hidaka in Commemoration of His Sixtieth Birthday*, ed. K Yoshida, pp. 53–58. Seattle: Univ. Wash. Press

Strub PT, Chereskin TK, Niiler PP, James C, Levine MD. 1997. Altimeter-derived variability of surface velocities in the California Current System: 1. Evaluation of TOPEX altimeter velocity resolution. *J. Geophys. Res.* 102:12727–48

Stum J. 1994. A comparison between TOPEX microwave radiometer, ERS 1 microwave radiometer, and European Centre for Medium Range Weather Forecasting derived wet tropospheric corrections. *J. Geophys. Res.* 99:24927–40

Sturges W. 1974. Sea level slope along continental boundaries. *J. Geophys. Res.* 79:825–30

Tapley BD, Reis JC, Davis GW, Eanes RJ, Schutz BE, et al. 1994. Precision orbit determination for TOPEX/POSEIDON. *J. Geophys. Res.* 99:24383–404

Tapley BD, Watkins MM, Ries JC, Davis GW, Eanes RJ, et al. 1996. The Joint Gravity Model 3 model. *J. Geophys. Res.* 101:28029–49

TOPEX Science Working Group. 1981. *Satellite Altimetric Measurements of the Ocean*. Natl. Aeronaut. Space Admin., Jet Prop. Lab., Calif. Inst. Technol., Pasadena. 78 pp.

Verron J, ed. 1992. Satellite Altimetry for Oceanography. *Oceanol. Acta Spec. Iss. (From Data Processing to Data Assimilation)* 15:407–583

Visbeck M, Marshall J, Haine T, Spall M. 1997. On the specification of eddy transfer coefficients in coarse resolution ocean circulation models. *J. Phys. Ocean.* 27:381–402

Wahr JM. 1988. The Earth's rotation. *Annu. Rev. Earth Planet. Sci.* 16:231–49

Walsh EJ, Jackson FC, Hines DE, Piazza C, Hevizi LG, et al. 1991. Frequency dependence of electromagnetic bias in radar altimeter sea surface measurements. *J. Geophys. Res.* 96:20571–83

Watts AB, McKenzie DP, Parsons BE, Roufosse M. 1985. The relationship between gravity and bathymetry in the Pacific Ocean. *Geophys. J.* 83:263–98

White MA, Heywood KJ. 1995. Seasonal and interannual changes in the North Atlantic subpolar gyre from Geosat and TOPEX/POSEIDON altimetry. *J. Geophys. Res.* 100: 24931–41

White WB, Peterson RG. 1996. An Antarctic circumpolar wave in surface pressure, wind, temperature and sea-ice extent. *Nature* 380:699–702

White WB, Tai C-K. 1995. Inferring interannual changes in global upper ocean heat storage from TOPEX altimetry. *J. Geophys. Res.* 100:24943–54

Wilkin J, Morrow RA. 1994. Eddy kinetic energy and momentum flux in the Southern Ocean: comparison of a global eddy-resolving model with altimeter, drifter and current-meter data. *J. Geophys. Res.* 99: 7903–16

Wunsch C. 1981a. An interim relative sea surface for the North Atlantic Ocean. *Mar. Geod.* 5:103–19

Wunsch C. 1981b. Low frequency variability of the sea. In *Evolution of Physical Oceanography: Scientific Surveys in Honor of Henry Stommel*, ed. BA Warren, C Wunsch, pp. 342–74. Cambridge: MIT Press

Wunsch C. 1989. Sampling characteristics of satellite orbits. *J. Atmos. Ocean. Technol.* 6: 891–907

Wunsch C. 1996. *The Ocean Circulation Inverse Problem.* Cambridge: Cambridge Univ. Press. 437 pp.

Wunsch C. 1997. The vertical partition of horizontal kinetic energy and the spectrum of global variability. *J. Phys. Ocean.* 27:1770–94

Wunsch C, Gaposchkin EM. 1980. On using satellite altimetry to determine the general circulation of the oceans with application to geoid improvement. *Rev. Geophys. Space Phys.* 18:725–45

Wunsch C, Stammer D. 1995. The global frequency-wavenumber spectrum of oceanic variability estimated from TOPEX/POSEIDON altimetric measurements. *J. Geophys. Res.* 100:24895–910

Wunsch C, Stammer D. 1997. Atmospheric loading and the "inverted barometer" effect. *Rev. Geophys.* 35:79–107

Zlotnicki V. 1994. Correlated environmental corrections in TOPEX/POSEIDON, with a note on ionospheric accuracy. *J. Geophys. Res.* 99:24907–14

Annual Review of Earth and Planetary Science
Volume 26, 1998

CONTENTS